Learning Linear Gaussian Polytree Models with Interventions

D. Tramontano[1], L. Waldmann[1], M. Drton[1], and E. Duarte[2]

[1]Technical University of Munich; School of Computation, Information and Technology, Department of Mathematics and Munich Data Science Institute, Germany
[2]Faculdade de Cincias, Universidade do Porto, Portugal

Abstract

We present a consistent and highly scalable local approach to learn the causal structure of a linear Gaussian polytree using data from interventional experiments with known intervention targets. Our methods first learn the skeleton of the polytree and then orient its edges. The output is a CPDAG representing the interventional equivalence class of the polytree of the true underlying distribution. The skeleton and orientation recovery procedures we use rely on second order statistics and low-dimensional marginal distributions. We assess the performance of our methods under different scenarios in synthetic data sets and apply our algorithm to learn a polytree in a gene expression interventional data set. Our simulation studies demonstrate that our approach is fast, has good accuracy in terms of structural Hamming distance, and handles problems with thousands of nodes.

1 Introduction

The dominant approach in recent literature on causal discovery from interventional data is optimization of a model score. Although the scoring is straightforward in the sense that the optimization over DAGs refers to fully specified joint models for all observational and interventional data, the optimization landscape is very high-dimensional, making score-based algorithms infeasible for graphs with hundreds/thousands of nodes that are common in biological applications. This makes causal discovery difficult, in addition to many other challenges that remain such as departing from restrictive genericity assumptions on the underlying distributions and developing methodology for high-dimensional settings. In this article, to address these challenges, we depart from a score-based strategy and leverage special properties of polytrees to obtain a highly scalable "local" approach that learns from low-dimensional marginals.

Our methods yield fast and consistent algorithms to learn linear Gaussian polytrees from interventional data. The skeleton is learned by aggregating pairwise correlations from different experimental settings; edge orientations are found by testing pairwise regression coefficients on suitable subsets of the data. This removes the need to form a score that contemplates joint models for all data. Moreover, we allow the intervention targets to be arbitrary subsets (with no variable always intervened upon). We are not aware of any other work with these features. While it will be interesting to seek extensions to broader classes of graphs in future work, we stress that for very high-dimensional problems (e.g., Dixit et al. [14]) it is of interest to target simpler computationally tractable objects that may be inferred reliably with moderate sample size [16]. For this reason, polytrees have received renewed interest.

2   Related work

Directed acyclic graphs (DAGs) have been extensively used in causal modeling; the nodes of a graph represent the random variables of the model while the directed edges represent causal effects from source to sink. The effects of the parent nodes on the children are quantified by structural equations. Causal discovery is then the problem of inferring the graphical structure underlying the model.

Approaches for causal discovery using only observational data and under the assumption that all variables in the model are directly observed/measured, include constraint-based, score-based and hybrid methods (e.g., PC-algorithm [47], Greedy Equivalent Search (GES) [9], Greedy SP algorithm [46]). Without extra assumptions on the data generating process, these methods learn a completed partially directed graph (CPDAG), a mixed graph that encodes the causal information common to all the members of a Markov equivalence class (MEC). Classical constrained-based algorithms, such as the PC algorithm, can suffer from the elevated number of conditional independence tests that are needed to learn the CPDAG. A recent line of work [2, 35, 37], which has proven to be almost optimal in terms of the number of conditional independence tests performed and is also applicable in the presence of unobserved variables, exploits the idea of learning the graph recursively starting from Markov boundary information.

Learning only the CPDAG is not always satisfactory as DAGs in the same MEC can have opposite causal interpretations. However, using additional assumptions such as non- Gaussianity [45] and/or non-linearity [27] it is possible to identify the complete causal structure. Whenever these assumptions do not apply, such as in the linear Gaussian case, additional data from interventional experiments can help to improve the identifiability of directed edges by refining the MEC. This refinement is quantified in terms of interventional Markov equivalence classes ($\mathcal{I}$-MECs) [56]. An $\mathcal{I}$-MEC is a collection of DAGs that entails the same interventional distributions for a fixed choice of intervention targets $\mathcal{I}$.

Within the causal discovery methods that use interventional data, there are those in which intervention targets are known such as Greedy Interventional Equivalent Search (GIES) [24], Interventional GSP (IGSP) [55], and Joint Causal Inference [38]. Other methods accommodate for unknown interventions targets, for instance Differentiable Causal Discovery with Interventions (DCDI) [6], permutation based approaches [49], and Bayesian Causal Discovery with unknown Interventions (BaCaDI) [23]. For a recent review of causal discovery methods we refer the reader to [48, 57].

In this paper, we address the problem of causal discovery when both observational and interventional data are available and all variables are measured. Our focus is on linear Gaussian structural causal models in which the graph is a polytree and the intervention targets are known. As shown computationally in [1], the polytree assumption provides an effective compromise between computational complexity and model expressiveness. This property of polytrees has been effectively exploited in image segmentation [18], hardware optimization [58], and Ozone prediction [50]. The polytree assumption follows a recent paradigm in the causal discovery literature in which assumptions are made about the DAG underlying the causal model in order to reduce the complexity of learning algorithms. Other methods that follow a similar approach include the causal additive trees (CAT) method which assumes the underlying DAG is a tree [29] and the method from [36] which incorporates side information such as the assumption that the ground truth is a diamond free graph or that an upper bound on the clique number of the graph is known.

The polytree assumption has been studied since the early days of causal reasoning theory. Indeed, Rebane and Pearl [41] use the Chow-Liu algorithm [10] to learn the skeleton of a polytree. Different variants of the Rebane and Pearl approach that work under different sets of assumptions have been developed in [33, 54, 8], a linear programming algorithm is developed in [32], while in [5] the graph is assumed to be locally a polytree around a targeted node allowing to infer the directed causes of the target node. Both Etesami et al. [17], in the context of time series graphs, and Sepehr and Materassi [44] in the context of classical graphical models, introduce a notion of minimality for polytrees with hidden nodes and provide an algorithm for learning the graph under the assumption of minimality. Polytree learning has been proven to be an NP-hard problem in [13], the complexity of the problem is studied in full details in [22]. In [4], a complete characterization is given for the constraints that emerge between 2nd and 3rd order moments of a random vector that follows a polytree-based linear structural equation model with non-Gaussian error terms.

3 Preliminaries

3.1 Notation for Graphs

A *directed graph* is a pair $G = (V, E)$, where V is the set of vertices and $E \subset \{(u, v) : u, v \in V, u \neq v\}$ is the set of directed edges. We denote a pair $(u, v) \in E$ also by $u \to v$. A *walk* from node v to node w in G is an alternating sequence $(v_0, e_1, v_1, e_2, \ldots, v_{k-1}, e_k, v_k)$ consisting of nodes and edges of G such that $v_0 = v$, $v_k = w$, and $e_l \in \{(v_{l-1}, v_l), (v_l, v_{l-1})\}$ for $l = 1, \ldots, k$. A walk is a *directed path* if $e_i = (v_{i-1}, v_i)$ for all $i \in \{1, \ldots, k\}$ and a *directed cycle* if additionally $v_0 = v_k$. From now on we assume that the graph G is a *DAG* (directed acyclic graph), i.e., G does not contain any directed cycles.

A node v_l is a *collider* on a walk as above if $e_{l-1} = (v_{l-1}, v_l)$ and $e_l = (v_{l+1}, v_l)$. Moreover, v_l is an *unshielded collider* if neither (v_{l-1}, v_{l+1}) or (v_{l+1}, v_{l-1}) belongs to E.

A walk that does not contain a collider is called a *trek* from v to w. Every trek contains a unique node v_l that splits the trek into two directed paths from v_l to v and from v_l to w, respectively. This node is the *top* of the trek. Note that the top may be equal to v or w, in which case one of the two directed paths is trivial consisting of a single node and no edge. A trek is *simple* if it does not contain repeated nodes.

If $u \to v \in E$, then u is a *parent* of v, and v is a *child* of u. If G contains a directed path from u to v, then u is an *ancestor* of v and v is a *descendant* of u. The set of parents, children, ancestors, and descendants of u are denoted by $\mathrm{pa}(u), \mathrm{ch}(u), \mathrm{an}(u), \mathrm{de}(u)$, respectively. The *skeleton* of a DAG is the undirected graph obtained by replacing each edge (u, v), by an undirected edge, denoted here by $\{u, v\}$.

A *mixed graph* is a triple $G = (V, E, U)$, where E is the set of directed edges defined as above, and $U \subset E \subset \{\{u, v\} : u, v \in V, u \neq v\}$ is the set of undirected edges. We assume all the graphs we consider to be *simple*, i.e., there is at most one edge, directed or undirected, between any two vertices.

3.2 Linear Structural Causal Models

Let $X = (X_u)_{u \in V}$ be a random vector indexed by the vertices of a DAG G. For $A \subset V$, let $X_A = (X_u)_{u \in A}$. When X_A is conditionally independent of X_B given X_C for disjoint subsets $A, B, C \subset V$, we write $A \perp\!\!\!\perp B \,|\, C$. The joint distribution of X satisfies the *local Markov property* with respect to G if $\{i\} \perp\!\!\!\perp [p] \setminus (\mathrm{pa}(i) \cup \mathrm{de}(i)) \,|\, \mathrm{pa}(i) \; \forall \, i \in [p]$. The Markov equivalence class of G is the set of all DAGs that encode the same conditional independence relations, i.e., for which the set of distributions satisfying the local Markov property is the same. See [34, Chap. 1] for further details.

The Gaussian structural causal model given by G postulates that

$$X_v = \sum_{w \in \mathrm{pa}(v)} \lambda_{wv} X_w + \varepsilon_v, \qquad v \in V, \tag{1}$$

where the edge coefficients $\lambda_{wv} \in \mathbb{R}$ are unknown parameters and the errors $(\varepsilon_v)_{v \in V}$ are independent Gaussian random variables. Each error is assumed to have mean zero and unknown variance $\omega_v > 0$; in symbols, $\varepsilon_v \sim \mathcal{N}(0, \omega_v)$. Let $\Lambda \in \mathbb{R}^{V \times V}$ be the matrix of edge coefficients, with zeros filled in at non-edges. Let $\Omega = \mathrm{diag}((\omega_v)_{v \in V}) \in \mathbb{R}^{V \times V}$ be the diagonal covariance matrix of $\varepsilon = (\varepsilon_v)_{v \in V}$. Solving (1), we obtain that $X = (I - \Lambda^T)^{-1} \varepsilon$ is a Gaussian random vector with covariance matrix

$$\Sigma := \mathrm{Var}[X] = (I - \Lambda^T)^{-1} \Omega (I - \Lambda)^{-1}, \tag{2}$$

we stress that the matrix $(I - \Lambda)$ is always invertible when the graph G is acyclic, this is because the matrix Λ is strictly lower triangular, so the determinant of $(I - \Lambda)$ is one.

As presented, X is modeled to have mean zero. This is without of loss of generality for the later results which solely pertain to the covariance structure. In the sequel, we denote the space of matrices supported on the edge set of G as

$$\mathbb{R}^E = \{\Lambda \in \mathbb{R}^{V \times V} : (v, w) \notin E \implies \Lambda_{vw} = 0\}.$$

We write D_+ for the set of diagonal matrices in $\mathbb{R}^{V \times V}$ with positive diagonal entries. The covariance model induced by the DAG G is the set of positive definite matrices

$$\mathcal{M}(G) := \{(I - \Lambda^T)^{-1} \Omega (I - \Lambda)^{-1} : \Lambda \in \mathbb{R}^E, \ \Omega \in D_+\}.$$

Two graphs G_1 and G_2 are *Markov equivalent* if and only if $\mathcal{M}(G_1) = \mathcal{M}(G_2)$ (see e.g. [42, Thm. 8.13]). Combinatorially, the MEC is represented by its CPDAG [34, Chap. 1].

Writing explicitly the entries of the a covariance matrix $\Sigma \in \mathcal{M}(G)$ using Eq. (2), one can get two useful parametrizations for the set $\mathcal{M}(G)$, we report the two parametrizations here, and refer to [51] and the references therein for further details.

Proposition 3.1 (Trek-rule)**.** *Let $\mathcal{T}(v, w)$ be the set of all treks from v to w. The matrix Σ from Eq. (2) has its entries*

$$\Sigma_{vw} = \sum_{\tau \in \mathcal{T}(v,w)} \omega_{\mathrm{top}(\tau)} \prod_{e \in \tau} \lambda_e, \quad v, w \in V.$$

Moreover, the entries of Σ satisfy the recursive relation

$$\Sigma_{vw} = \sum_{\tau \in \mathcal{S}(v,w)} \Sigma_{\mathrm{top}(\tau),\mathrm{top}(\tau)} \prod_{e \in \tau} \lambda_e, \quad v, w \in V,$$

where $\mathcal{S}(v, w)$ is the set of simple treks from v to w.

Let $\Sigma = (\sigma_{vw})$ be the covariance matrix of a random vector X, with diagonal entries $\sigma_{vv} > 0$. The correlation matrix $R(\Sigma) = (\rho_{vw})$ of Σ is the matrix with entries $\rho_{vw} = \sigma_{vw}/\sqrt{\sigma_{vv}\sigma_{ww}}$. It is also the covariance matrix of the standardized random vector $(X_v/\sqrt{\sigma_{vv}})_{v \in V}$.

Proposition 3.2 (Correlation matrices)**.** *If Σ is a covariance matrix in $\mathcal{M}(G)$, then its correlation matrix $R(\Sigma)$ is also in $\mathcal{M}(G)$. Hence, there exists $\Lambda = (\lambda_{vw}) \in \mathbb{R}^E$ such that*

$$R(\Sigma)_{vw} = \sum_{\tau \in \mathcal{S}(v,w)} \prod_{e \in \tau} \lambda_e, \quad v, w \in V.$$

Proof. Write $\Sigma = (I - \Lambda')^{-T} \Omega' (I - \Lambda')^{-1}$ for $\Lambda' \in \mathbb{R}^E$ and $\Omega' \in D_+$. Then $R(\Sigma) = (I - \Lambda^T)^{-1} \Omega (I - \Lambda)^{-1}$, where the entries of $\Lambda \in \mathbb{R}^E$ are $\Lambda_{vw} = \Lambda'_{vw} \sqrt{\Sigma_{vv}}/\sqrt{\Sigma_{ww}}$ and those of $\Omega \in D_+$ are $\Omega_{vv} = \Omega'_{vv}/\Sigma_{vv}$.

The second assertion follows from the simple trek-rule in Proposition 3.1, observing that $R(\Sigma)_{vv} = 1$ for all v. $\qquad\square$

3.3 Interventions

It is useful to formally consider the collection of linear Gaussian structural causal models that arise from G and a set of interventions. In a *soft intervention*, a subset $I \subset V$ of target nodes is selected, and for each $v \in I$ the conditional distribution of X_v given $X_{\mathrm{pa}(v)}$ is modified. When X_v is made independent of its parents, the intervention is *perfect*. It is common that different interventions are performed and hence we have a collection of intervention targets denoted by $\mathcal{I}$, so $\mathcal{I} \subseteq 2^V$. Without loss of generality we assume that $\emptyset \in \mathcal{I}$ and refer to this as the observational experiment. Theorem 3.14 in Yang et al. [56] justifies this assumption, which subsumes the case of conservative intervention targets treated by Hauser and Bühlmann [24].

We assume that each interventional experiment obeys a linear Gaussian structural causal model defined by G (recall Section 3.2). Namely, for each $I \in \mathcal{I}$, we have a random vector $X^I := (X_v^{(I)})_{v \in V}$ with structural equations

$$X_v^{(I)} = \sum_{w \in \mathrm{pa}(v)} \lambda_{wv}^{(I)} X_w^{(I)} + \varepsilon_v^{(I)}, \qquad v \in V. \tag{3}$$

We use $\Lambda^{(I)}$ to denote the matrix of edge coefficients for this model and $\Omega^{(I)} = \mathrm{diag}((\omega_v^{(I)})_{v \in V})$ to denote the covariance matrix of the Gaussian vector $\varepsilon^{(I)} := (\varepsilon_v^{(I)})_{v \in V}$. To encode the invariances of the structural equations of nodes that are not intervened on, i.e are not in I, we impose that $\lambda_{wv}^{(I)} = \lambda_{wv}^{(\emptyset)}$ and $\omega_v^{(I)} = \omega_v^{(\emptyset)}$ whenever $v \notin I$. Each I induces a covariance model

$$\mathcal{M}(G, I) = \{\Sigma^{(I)} : \Lambda^{(I)} \in \mathbb{R}^E, \Omega^{(I)} \in D_+\}$$

where $\Sigma^{(I)} = (I - (\Lambda^{(I)})^T)^{-1} \Omega^{(I)} (I - \Lambda^{(I)})^{-1}$ and $\Lambda^{(I)}, \Omega^{(I)}$ satisfy the invariances, on edge coefficients and error variances, of nodes that are not intervened on.

The interventional DAG model specified by G and the set of intervention targets $\mathcal{I}$ is the set

$$\mathcal{M}_{\mathcal{I}}(G) := \{(\Sigma^{(I)})_{I \in \mathcal{I}} : \Sigma^{(I)} \in \mathcal{M}(G, I), I \in \mathcal{I}\};$$

it consists of tuples of covariance matrices of length $|\mathcal{I}|$ that may arise by performing interventions according to $\mathcal{I}$.

Two DAGs G_1, G_2 are in the same $\mathcal{I}$-*Markov equivalence class*, $\mathcal{I}$-MEC, if and only if $\mathcal{M}_{\mathcal{I}}(G_1) = \mathcal{M}_{\mathcal{I}}(G_2)$. To decide if two DAGs are in the same $\mathcal{I}$-MEC, Yang et al. [56] introduce the notion of an $\mathcal{I}$-DAG:

Definition 3.1 ($\mathcal{I}$-DAG). *Fix a collection of interventions $\mathcal{I}$ and a DAG G, the $\mathcal{I}$-DAG $G^{\mathcal{I}}$ is the graph G augmented with $\mathcal{I}$-vertices $\{\zeta_I\}_{\emptyset \neq I \in \mathcal{I}}$, and the $\mathcal{I}$-edges $\{\zeta_I \to u\}_{u \in I, I \in \mathcal{I}}$.*

The following theorem provides a concise graphical representation of the $\mathcal{I}$-*Markov equivalence classes*.

Theorem 3.3. *[56, Thm. 3.14] Let $\mathcal{I}$ be a conservative set of intervention targets. Two DAGs G_1, G_2 are in the same $\mathcal{I}$-MEC iff for all $I \in \mathcal{I}$ the $\mathcal{I}$-DAGs $G_1^{\tilde{\mathcal{I}}_I}$ and $G_2^{\tilde{\mathcal{I}}_I}$ have the same skeleton and the same v-structures, where*

$$\tilde{\mathcal{I}}_I = \{\emptyset\} \cup \{I \cup J\}_{I, J \in \mathcal{I}, I \neq J}.$$

The $\mathcal{I}$-MEC of a DAG G can be represented uniquely by its $\mathcal{I}$-CPDAG, this provides a combinatorial representation of the causal information that we can extract from the interventional data available, often also referred to as the $\mathcal{I}$-essential graph in the literature. This is a mixed graph with the same skeleton as G, a directed edge, (u, v), if every member of the $\mathcal{I}$-MEC has that edge with the same orientation, and an undirected edge, $\{u, v\}$, if there are two DAGs in the $\mathcal{I}$-MEC for which that edge has opposite orientations. See Hauser and Bühlmann [24, Thm. 18] for details in the setting of perfect interventions, the same construction carries over to the setting of general interventions [56].

4   Learning Causal Models on Polytrees with Interventions

From now on we assume that the DAG G is a polytree, this means that the skeleton of G is a tree, i.e., a graph in which there is exactly one path between any two nodes.

Our procedure first learns the skeleton. For this purpose we create a novel interventional version of the Chow-Liu algorithm [10]. The challenge here lies in constructing a weight matrix that reveals the tree structure, the same way the correlation matrix on a single observational data set does. As seen in Fig. C.1, taking simply the correlation matrix of the pooled data does not work. Thus, we introduce the notion of a G-valid weight matrix that suitably captures the tree structure. We will construct G-valid weight matrices by aggregating correlation matrices. The aggregation does not necessarily produce a correlation matrix, yet we show that this approach yields a consistent procedure to learn the skeleton in low- and high-dimensional settings. The approach is detailed in Section 4.1. Its consistency is discussed in Appendix A.1.

To determine the orientation of the edges we propose and compare several methods described in Sections 4.3 and 4.4; their consistency is discussed in the Appendix A. Importantly, all procedures use only correlations and low-dimensional marginal distributions that are efficiently estimable in a low sample regime, see e.g., the concentration inequality given in [30, Cor. 1] in which it is explicit that the effective sample size decreases as the size of conditioning set increases requiring more samples to achieve the same accuracy in the estimation.

4.1   Learning a Skeleton

In seminal work, Rebane and Pearl [41] proved that when a distribution satisfies conditional independence constraints induced by a polytree, then the skeleton of the tree can be recovered using the

algorithm for the maximum weight spanning tree of Kruskal [31], with weight matrix given by the mutual information between the variables. Notably, the only property of mutual information needed in this algorithm is the data processing inequality [12, Thm. 2.8.1]. This implies that Kruskal's algorithm finds the correct polytree skeleton any time the weight matrix that is used respects the following condition.

Definition 4.1. *Given a polytree G, a weight matrix $W \in \mathbb{R}^{p \times p}$ is G-valid if for every triplet $u - v - w$ in G*

$$\min\{W(u,v), W(v,w)\} \geq W(u,w). \tag{4}$$

If all inequalities in (4) are strict, then W is strictly G-valid.

Lemma 4.1. *[41, Thm. 1] If W is strictly G-valid, then the maximum weight spanning tree of the complete graph over V with weight matrix W is the skeleton of G.*

In a polytree G there is at most one trek between any two vertices. In particular for any triple $u - v - w$, the only possible trek between u and w is the one involving also v, so from Proposition 3.2 we have that $|\rho_{u,w}| = 0$ if $u - v - w$ is a collider triple and $|\rho_{u,w}| = |\rho_{u,v}||\rho_{v,w}|$ otherwise. In particular, the absolute (observational) correlations define a G-valid weight matrix that is strictly G-valid if G is causally minimal. Similarly, for each $I \in \mathcal{I}$, the associated absolute correlation matrix $|R^I|$ is a G-valid weight matrix.

To efficiently learn from available interventional data, we wish to form a single weight matrix that encodes the information of all the experimental settings. To this end, we use an aggregation function $A : (\mathbb{R}^{p \times p})^{|\mathcal{I}|} \to \mathbb{R}^{p \times p}$ that takes a collection of G-valid weight matrices and outputs a strictly G-valid matrix. One way of obtaining such a function A is to apply the same order-preserving transformation $a : \mathbb{R}^{|\mathcal{I}|} \to \mathbb{R}$ to each vector of correlations $(\rho_{ij}^1, \ldots, \rho_{ij}^{|\mathcal{I}|})$. By order-preserving, we mean that $a(x_1, \ldots, x_{|\mathcal{I}|}) \leq a(y_1, \ldots, y_{|\mathcal{I}|})$ anytime $x_i \leq y_i$ for $i = 1, \ldots, |\mathcal{I}|$. Possible choices for a are:

1. $a(\rho_{ij}^1, \ldots, \rho_{ij}^{|\mathcal{I}|})) = -\sum_{I \in \mathcal{I}} \frac{n_I}{2} \log(1 - (\rho_{ij}^I)^2),$[1]

2. Weighted mean,

3. Weighted median,

where n_I is the size of the dataset I and the weights we refer to for the mean and the median are $\frac{n_I}{\sum n_I}$.

The output of Kruskal's algorithm is the same for any strictly G-valid matrix W. In practice, however, we work with an estimate $\tilde{W}$ and different aggregation functions can give different results. We discuss the numerical performance of the three aggregation functions in Section 5.1.

4.2 Identifiability of Edge Orientations

The output of our learning methods is an $\mathcal{I}$-CPDAG (Section 3.3) whose construction simplifies for polytrees. The next definition singles out the edge directions that can be identified in a polytree. Notice that in a polytree there is only one path between two vertices, thus all the colliders are unshielded.

Definition 4.2. *An edge $u \to v \in G$ is $\mathcal{I}$-directly-identifiable if it is either part of a collider, or there exists $I \in \mathcal{I}$ such that $|I \cap \{u,v\}| = 1$. It is $\mathcal{I}$-identifiable if it is either $\mathcal{I}$-directly-identifiable, or there is an edge $w \to u \in E$ that is $\mathcal{I}$-identifiable.*

Proposition 4.2. *The $\mathcal{I}$-CPDAG of G is the partially directed graph that has the same skeleton of G, and whose directed edges are the edges of G that are $\mathcal{I}$-identifiable.*

It is clear from Definition 4.2 that once we have computed the skeleton of the polytree, the $\mathcal{I}$-CPDAG can be identified by searching the $\mathcal{I}$-directly-identifiable edges first. Then, once we have a triple of the form $u \to v - w$ we can orient $v - w$ testing if the triple forms a collider. In the next sections we describe different orientiation strategies: Section 4.3 focuses on single edge orientations, and Section 4.4 focuses on finding colliders. Searching for one type of $\mathcal{I}$-directly-identifiable edge or the other first does

---

[1]This is well defined for absolute correlations in $[0, 1)$.

not matter on a population level. However, it can make a difference when working with data due to approximation errors inherent to each possible approach. A comparison of performance between these approaches is given in Appendix C.3.

Hereafter, X_u^I, X_v^I denote vectors of observed values of the variables X_u, X_v in the interventional setting $I \in \mathcal{I}$. Entrywise, $X_u^I = (X_{u,1}^I, \ldots, X_{u,n_I}^I)$ and $X_v^I = (X_{v,1}^I, \ldots, X_{v,n_I}^I)$. The total sample size is then $n := \sum_{I \in \mathcal{I}} n_I$. Fix $\mathcal{I}$ and an edge $\{u, v\}$, we define

$$\mathcal{I}_{\dot{v}} := \{I \in \mathcal{I} : v \notin I\}, \qquad\qquad \mathcal{I}_{\dot{u},v} := \{I \in \mathcal{I} : v \in I, u \notin I\},$$
$$\mathcal{I}_{\dot{u},\dot{v}} := \{I \in \mathcal{I} : u, v \notin I\}, \qquad\qquad \mathcal{I}_{u,\dot{v}} := \{I \in \mathcal{I} : u \in I, v \notin I\}.$$

4.3 Learning Single Edge Orientations

4.3.1 Invariance of Regression Coefficients (IRC)

To orient the edge $\{u, v\}$, we assume there exists $I_0 \in \mathcal{I}$ where no intervention took place, i.e., $I_0 = \emptyset$. Fix $I \in \mathcal{I}_{u,\dot{v}}$. If the true model is $u \to v$, then an intervention on u does not change the regression coefficient of $X_v^I = \lambda_{uv}^I X_u^I + \epsilon^I$, $\epsilon^I \sim \mathcal{N}(0, \sigma_{v|u})$. Namely, $\lambda_{uv}^I = \lambda_{uv}^\emptyset$. Thus to orient the edge $\{u, v\}$ we test the hypothesis $\mathcal{H} : \lambda_{uv}^I = \lambda_{uv}^\emptyset$. There are different options for the choice of this test and IRC testing has been used before in causal structure learning [e.g., 26, 20]. Here we use an F-test [52], which is a modified version of the test statistic in [11] for the case of unequal variances. We briefly present it here.

Let e_{I_0} and e_I denote the vectors of residuals of the regressions $X_v^I = \lambda_{uv}^{I_0} X_u^{I_0} + \epsilon^{I_0}$ and $X_v^I = \lambda_{uv}^I X_u^I + \epsilon^I$ respectively, and let e denote the vector of residuals, which is obtained by pooling the data sets $(X_u^{I_0}, X_v^{I_0}), (X_u^I, X_v^I)$. Under the null hypothesis $\mathcal{H}_{I, u \to v}$ the statistic is

$$\frac{(e^T e - e_{I_0}^T e_{I_0} - e_I^T e_I)/k}{(e_{I_0}^T e_{I_0} - e_I^T e_I)/f} \sim F(k, f)$$

where $k = 2$ and $f = \frac{((n_{I_0} - k)\hat{\sigma}_{I_0}^2 + (n_I - k)\hat{\sigma}_{I_0})^2}{(n_{I_0} - k)\hat{\sigma}_{n_0}^4 + (n_I - k)\hat{\sigma}_{n_I}^4}$.

For each $I \in \mathcal{I}_{u,\dot{v}}$ we test the hypothesis $\mathcal{H}_{I, u \to v}$ and reject the orientation $u \to v$ in favor of $v \to u$ if the p-value of any of these tests is below $\alpha/|\mathcal{I}_{u,\dot{v}}|$ for some chosen significance level α. This test is possible whenever $\mathcal{I}_{u,\dot{v}} \neq \emptyset$.

In an analogous fashion, changing the roles of u, v, if $\mathcal{I}_{\dot{u},v}$ is nonempty, we may perform a test for the orientation $v \to u$. If only one of the tests $u \to v$ or $v \to u$ is possible, then the decision rule to orient the edge $\{u, v\}$ is clear. In case both tests are possible, we choose to reject the test with the smallest p-value, as long as such p-value is below the corresponding significance ($\alpha/|\mathcal{I}_{u,\dot{v}}|$ or $\alpha/|\mathcal{I}_{\dot{u},v}|$).

4.3.2 Single Edge BIC Score Before Collider Search

Let $\mathcal{H}_1$ and $\mathcal{H}_2$ be any two parametric models with parameter spaces $\mathcal{M}_1 \subset \mathbb{R}^{r_1}$ and $\mathcal{M}_2 \subset \mathbb{R}^{r_2}$ and of dimensions d_1 and d_2, respectively. A model selection based on the BIC consists of choosing the minimizer of the following penalized log-likelihood

$$l(\mathcal{H}_i \mid X_n) = \underset{\theta_i \in \mathcal{M}_i}{\arg\min} \left(-\log(p_{\mathcal{H}_i}(X_n \mid \theta_i)) + \frac{d_i}{2} \log(n) \right), \tag{5}$$

for $i \in \{1, 2\}$, where X_n is the observed dataset of size n. For more details on model selection and information criteria, we refer the reader to [7, Chap. 2].

In our setting we want to select between the model in which $u \to v \in G$ and the one in which $v \to u \in G$, respectively denoted as $\mathcal{H}_{u \to v}$ and $\mathcal{H}_{v \to u}$. The polytree assumption allows us to compute the log likelihood using only information on the marginal distribution of u and v. We show in detail only the derivation of the penalized log likelihood for $\mathcal{H}_{u \to v}$, since the one for the other model is analogous.

Under the model $\mathcal{H}_{u \to v}$ we can write in each dataset $X_v = \lambda_{u,v}^I X_u + \epsilon_{v|u}^I$ where, using Eq. (3), we can see that

$$\epsilon_{v|u}^I = \sum_{w \in \mathrm{pa}(v) \backslash \{u\}} \lambda_{wv}^{(I)} X_w^{(I)} + \varepsilon_v^{(I)} \sim \mathcal{N}(0, \sigma_{v|u}^I), \tag{6}$$

$$\sigma_{v|u}^I = \sum_{w \in \mathrm{pa}(v) \backslash \{u\}} (\lambda_{wv}^2)^{(I)} \sigma_w^{(I)} + \sigma_v^{(I)}, \tag{7}$$

a consequence of the polytree is assumption is that X_u is independent from all the other parents of v, and so it is independent from $\epsilon_{v|u}$ as well. This allows us to rewrite the log-likelihood of a observed pair $(X_{u,i}^I, X_{v,i}^I)$ as

$$-\log 2\pi - \frac{1}{2} \log \sigma_u^{I\,2} - \frac{1}{2} \log \sigma_{v|u}^I{}^2 - \frac{(X_{u,i}^I)^2}{2\sigma_u^{I\,2}} - \frac{(X_{v,i}^I - \lambda_{u,v}^I X_{u,i}^I)^2}{2\sigma_{v|u}^I{}^2}.$$

The log-likelihood for the whole dataset is then

$$-n \log 2\pi + \sum_{I \in \mathcal{I}} \left(-\frac{n_I}{2} \log \sigma_u^{I\,2} - \frac{n_I}{2} \log \sigma_{v|u}^I{}^2 + \sum_{i \in [1, \ldots, n_I]} -\frac{(X_{u,i}^I)^2}{2\sigma_u^{I\,2}} - \frac{(X_{v,i}^I - \lambda_{u,v}^I X_{u,i}^I)^2}{2\sigma_{v|u}^I{}^2} \right). \tag{8}$$

Straightforward computations show that the MLEs for the variance parameters are the usual variances computed on each dataset individually leading to

$$\hat{\sigma}_u^{I\,2} = \frac{1}{n_I} \|X_u^I\|^2, \qquad\qquad \hat{\sigma}_{v|u}^{I\,2} = \frac{1}{n_I} \|X_v^I - \lambda_{u,v}^I X_u^I\|^2. \tag{9}$$

For the regression coefficients, since we know that they vary only across the datasets in which v has been intervened upon, it is not possible to find a closed form expression for the estimator. To handle this, we tell apart the datasets in which v has been intervened on from those in which it has not. Define $\lambda_{u,v}$ as the regression coefficient that is shared across the environments in which v has not been intervened on. Substituting (9) into (8), the part of the log-likelihood that depends on the regression coefficients becomes

$$-\left(\sum_{I \in \mathcal{I}_{\dot{v}}} \frac{n_I}{2} \log \|X_v^I - \lambda X_u^I\|^2 + \sum_{I \in \mathcal{I}_v} \frac{n_I}{2} \log \|X_v^I - \lambda^I X_u^I\|^2 \right).$$

So if $I \in \mathcal{I}_v$ then $\hat{\lambda}^I = (X_u^I \cdot X_v^I)/\|X_u^I\|^2$, while $\hat{\lambda}$ is given by the solution of the 1-dimensional bounded optimization problem

$$\arg\max_{\lambda \in [-1,1]} -\sum_{I \in \mathcal{I}_{\dot{v}}} \frac{n_I}{2} \log \|X_v^I - \lambda X_u^I\|^2. \tag{10}$$

For solving this problem, we find Brent's method, see e.g. [39, Chap. 10.3], to work well in practice. Finally, note that the dimension of the model, that is, the number of free parameters we need to optimize over, is $2|\mathcal{I}| + 1 + |\mathcal{I}_v|$. Indeed, we have two variance coefficients for each interventional dataset, one regression coefficient for the datasets in which v has not been intervened upon, and one regression coefficient for each dataset in which v has been intervened on.

Remark 4.1. In this section we allow the marginal variances σ_u and $\sigma_{v|u}$ to vary also in the datasets in which u and v are not intervened upon. This is because the variance can change also as a consequence of an intervention on an ancestor. A precise likelihood computation would require to check for each experiment if there are possible ancestors in the graph that can affect the marginal variances, but this would be too computationally expensive while giving little benefit in terms of likelihood comparison. We discuss this aspect further in the appendix, Prop. A.4, where we also clarify that consistency is not affected by the relaxation of the variance constraints.

4.3.3 Single Edge BIC Score After Collider Search

Let $G^{CP} = (V, E^{CP})$ be the CPDAG associated to G and G^U be graph obtained from G^{CP} after removing all the oriented edges. We can then work on each connected component of G^U independently. Let U be one of these components, and $u - v$ be one of its $\mathcal{I}$-directly-identifiable edges. If we orient the edge from u to v then we would orient the remaining edges in U in such a way that no other colliders appear. We now propose a simple likelihood computation that takes this into account.

The choice of an orientation for the edges in U reduces to the choice of a root vertex in it. If u is a vertex in U, then we let $\mathcal{H}_u^U$ denote the model in which u is the root. The likelihood function for this model factorizes in a simple way since each vertex has at most one parent. We can write the log-likelihood of a datapoint as

$$\log f(X_U^I) = \log f(X_u^I) + \sum_{v \neq u} \log f(X_v^I | X_{pa(v)}^I),$$

where each of the summands can be maximized independently from the others. This time the maximization is easier than the one in Section 4.3.2 because the variance parameters are shared across all environments in which a node has not been intervened upon. A closed form solution for this problem is provided in [25] and is given by $\hat{\sigma}_{v|\,pa(v)}^2 = \sum_{I_{\dot{v}}} \frac{n_I}{n_{\dot{v}}} \hat{\sigma}_{v|\,pa(v)}^{I^2}$, where $n_{\dot{v}} = \sum_{I_{\dot{v}}} n_I$ and $\hat{\sigma}_{v|\,pa(v)}^{I^2}$ is the MLE of the conditional variance in the dataset I, while $\hat{\lambda} = \frac{\hat{\sigma}_{v,pa(v)}}{\hat{\sigma}_{pa(v)}^2}$. The dimension of the model $\mathcal{H}_u$ is $1 + |\mathcal{I}_u| + 2\sum_{v \neq u}(1 + |\mathcal{I}_v|)$.

4.4 Collider Search

4.4.1 BIC Score for Collider Search

If the skeleton has a triplet $u - v - w$, we can decide whether it forms a collider or not by testing for the independence of u and w in all the environments. Log-likelihood ratio statistics for a test are provided by function 1 defined in Section (4.1), applied to $x_I = \rho_{u,w}^I$. Here the difference in the dimension between the model $\mathcal{H}_{u \to v \leftarrow w}$ and the other 3 models in which u and w are not independent is $|\mathcal{I}|$.

4.4.2 BIC Score for Collider Completion

Even though testing for the independence of u and w as in Section 4.4.1 would give a consistent procedure also in the case in which we have already oriented $u \to v$, in this case a more refined analysis of the likelihood is possible. Indeed, here we can test the model $u \to v \to w$ against $u \to v \leftarrow w$. In the former case the likelihood factorizes as $f(X_u^I)f(X_v^I|X_u^I)f(X_w^I|X_v^I)$ and can be maximized as in Section 4.3.2. In the latter case it factorizes as $f(X_u^I)f(X_w^I)f(X_v^I|X_u^I, X_w^I)$, and the MLE for $\lambda_v^I = (\lambda_{v|u}^I, \lambda_{v|w}^I)$ in the environments in which v has been intervened upon is given by the usual estimator $\hat{\Sigma}_{u,w}^{I^{-1}}\hat{\Sigma}_{v|u,w}^I$, while the common regression coefficients for the environments in which v hasn't been intervened on $\hat{\lambda}_{v|w}, \hat{\lambda}_{v|u}$, is given by the solution of the following 2 dimensional optimization problem:

$$\underset{\lambda_{v|u}, \lambda_{v|u} \in [0,1]^2}{\arg\max} \sum_{I \in \mathcal{I}_{\dot{v}}} -\frac{n_I}{2} \log ||X_v^I - \lambda_{v|u} X_u^I - \lambda_{v|w} X_w^I||^2$$

The dimension of the model $\mathcal{H}_{u \to v \to w}$ is $3|\mathcal{I}| + |\mathcal{I}_v| + |\mathcal{I}_w| + 2$ while that of the model $\mathcal{H}_{u \to v \to w}$ is $2(2|\mathcal{I}| + |\mathcal{I}_v| + 1)$.

4.5 Complete Orientation Procedures

We propose two procedures for the orientation. The pseudocode for each, including subroutines, is in Appendix B:

P.1 Compute the CPDAG using the collider search, then use single edge orientation.

P.2 Use single edge orientation first, then orient the rest of the $\mathcal{I}$-CPDAG using the collider search.

These procedures differ in the amount of statistical vs. causal information they extrapolate from data, with P.1 being the more statistically oriented, while P.2 the more causally oriented. Note that for the single edge orientation we can choose between BIC (Sec. 4.3.2) and IRC (Sec. 4.3.1), and to find colliders we can use the more general setting of Section 4.4.1 hereon referred to as "simple", or the more refined analysis of Section 4.4.2 hereon referred to as "refined".

Whenever we use the orientation procedures involving a BIC score, it is intended that we solve a local model selection problem in the following way: we compute the MLE estimator for the possible models (e.g., $\mathcal{H}_{u \to v}$ and $\mathcal{H}_{v \to u}$ for the single edge orientation) and then plug it into the likelihood function to compute the maximum likelihood $\hat{L}$, the BIC score of the model $\mathcal{H}$ will be $\log(n) \dim(\mathcal{H}) - 2 \log(\hat{L})$, where n is the sample size. Finally, we select the model with the highest BIC score.

5 Simulation Studies

In this section we first assess the performance of the different skeleton and orientation recovery procedures, then we construct full versions of our algorithms to compare to other methods. The setup for our simulations is explained in Appendix C.1, the code is available at [53].

5.1 Skeleton and Orientation Recovery

Fig. 1 shows the structural Hamming distance (SHD) in skeleton recovery for the three aggregation functions introduced in Section 4.1. The SHD is the minimum number of edge additions, deletions and reversals necessary to transform one graph into another. We see that the SHD decreases for increasing number of samples, with little effect of the number of datasets and the size of the intervention. Fig. C.2 in Appendix C.3. shows that the weighted mean is the fastest. A more detailed analysis is contained in Appendix C.2.
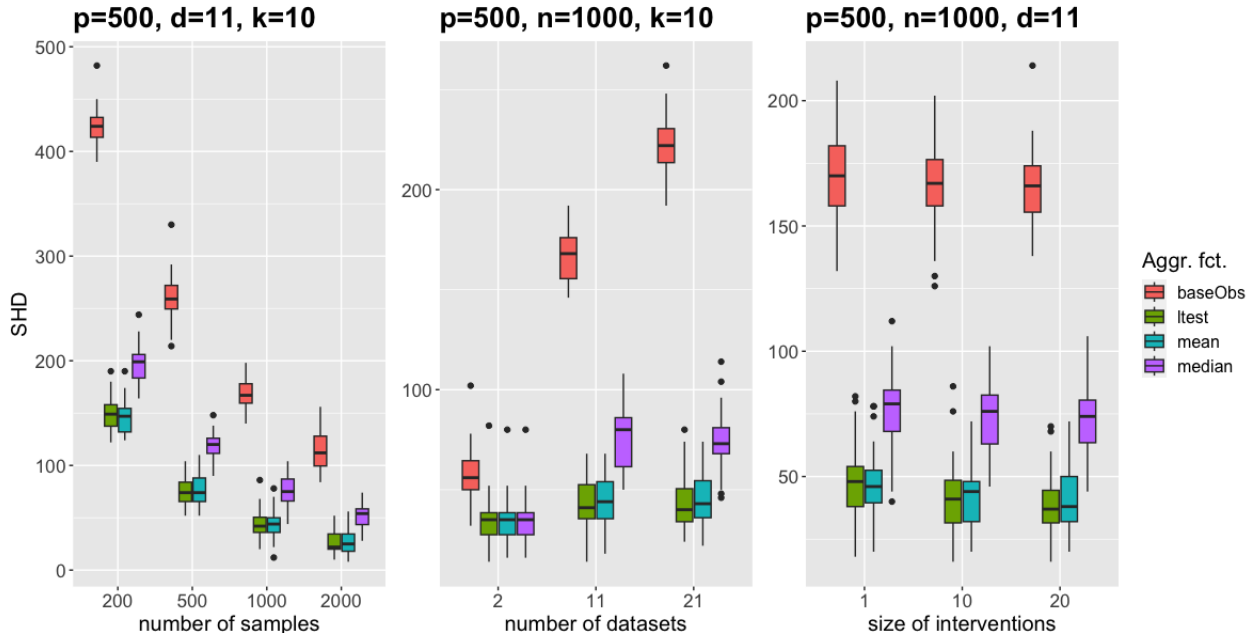

Figure 1: Skeleton recovery with $p = 500$ nodes, $N = 200, 500, 1000, 2000$ samples, $d = 2, 11, 21$ datasets (1 interventional and $d-1$ observational) and $k = 1, 10, 20$ nodes targeted per intervention, respectively. The aggregation function baseObs denotes a baseline with observational data only. The labels Itest, mean, median indicate each of the procedures in the list in Section 4.1 respectively.

Fig. 2 depicts the SHD in orientation recovery, conditional on the skeleton being correct. Inter-

estingly, the more refined test proposed in Section 4.4.2 gives no benefits compared to the ones in Section 4.4.1, and it is slower to compute. P.1 also performs better than P.2 in general. More details on the orientation procedure in Appendix C.3.

Remark 5.1. Notice that in the experiment shown in the middle panels of Figs. 1 and 2, the overall sample size is fixed, so increasing d significantly reduces the sample size in each one of the datasets, resulting in a much more difficult learning problem. This explains why the orientation procedures seem to be negatively affected by the introduction of interventional datasets.
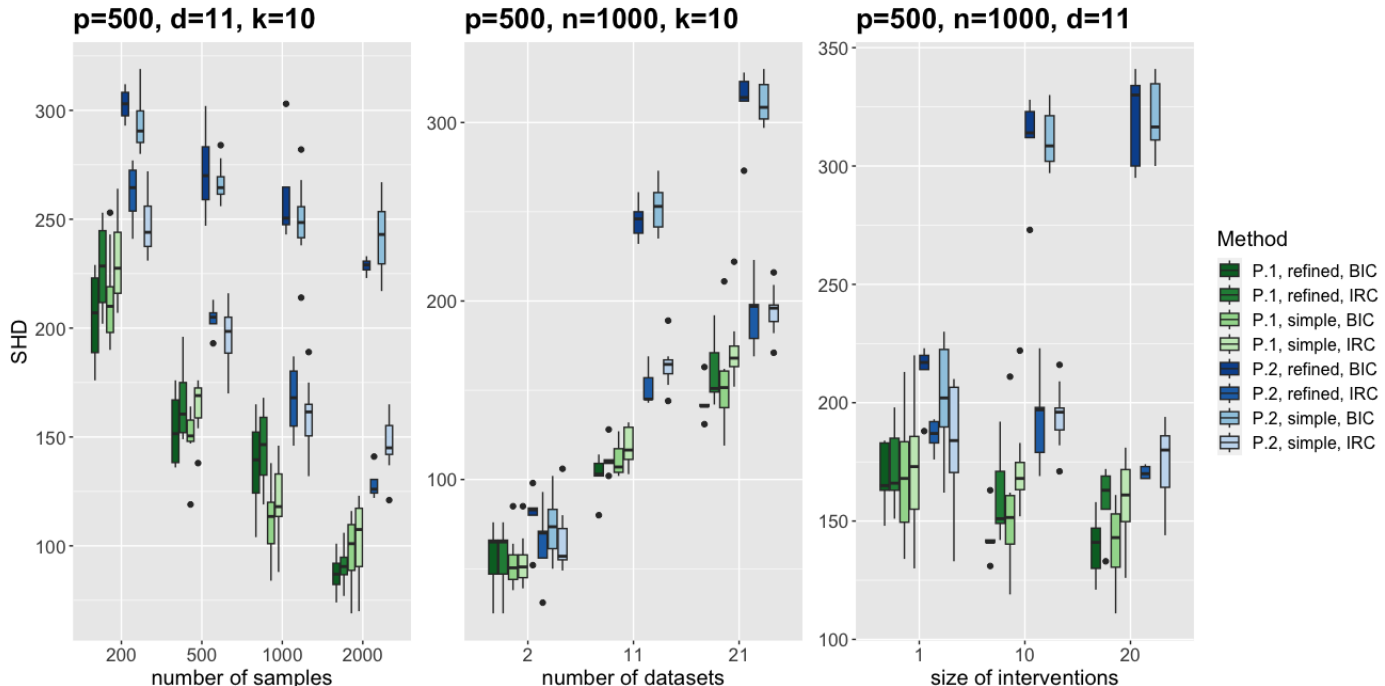
Figure 2: Orientation recovery with base parameters 500 nodes, 1000 samples and 10 intervention targets with 10 intervened nodes each. For all proposed methods we see the convergence when the sample size increases. In this case increasing the number of datasets negatively affects the performance, this point is disccused in Rem. 5.1.

5.2 Complete Algorithm

Although our focus is on causal discovery in high-dimensional settings, for completeness, we compare the performance of our full skeleton and orientation recovery procedures (Sec. 4.5) to the performance of GIES [24], DCDI [6], BaCaDI [23] and IGSP [55] in low dimension with simulations on DAGs with $p = 20$ nodes. The results are summarized in Fig. 3 (left). We see that general algorithms achieve a better accuracy, but this comes with a high price in terms of running time that makes them infeasible for larger graphs. We refer to Table C.2 for a runtime analysis.

For high-dimensional settings, to leverage accuracy and fast computation, we construct our full algorithm using either P.1 or P.2 with mean as aggregation function, simple for collider search and IRC for single edge orientations. Among the four algorithms from the literature considered in Fig. 3 (left), the only one that would terminate in less than 24h for DAGs with $p = 500$ nodes is GIES [25]. Thus, we compare our two high-dimensional versions of the algorithm with GIES only. The Fig. 3 (right) shows the results of the simulations. We see in this setting that our algorithm provides better accuracy in terms of structural Hamming distance in addition to being considerably faster, as the computation
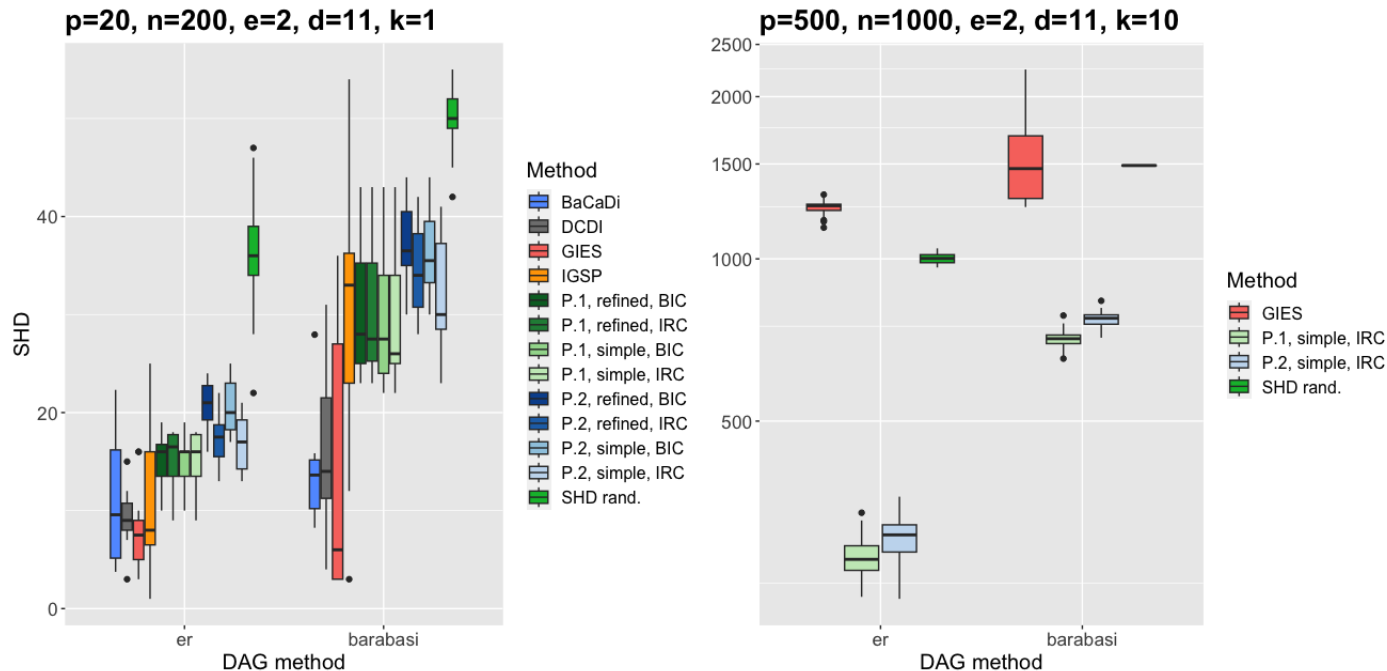
Figure 3: Performance of our algorithm against different baselines in low- and high-dimensional settings on DAGs for random Erdős-Rényi or Barabasi-Albert graphs with $p = 20, 500$ nodes and expected number of edges per node $e = 2$. The observational sample sizes are respectively 100 and 48, the other samples are evenly distributed in the interventional datasets. Notice that the y-axis for the plot on the right is in log-scale.

times in Table 1 indicate. Appendix C.5 contains an extensive comparison of our algorithm against GIES.

To emphasize the point that our algorithms are able to retain structural information of the original DAG, in both the plots in Fig. 3 we added "SHD rand." as baseline. This shows the SHD between the $\mathcal{I}$-CPDAG of the true DAG and the $\mathcal{I}$-CPDAG of randomly generated polytree. This baseline makes sure to highlight that the better performance of our algorithms in terms of SHD is not given by the sparsity structure of the polytree. The distance from the result of our algorithm to this baseline is a strong indication that even in a misspecified setting where the generating graph is not a polytree, our algorithms are still able to infer information about the original DAG.

Table 1: Mean runtime on DAGs with 500 nodes and different number of samples n corresponding to Fig. 3.

| Method | Runtime in seconds | | | | | |
| | $n = 500$ | | $n = 1000$ | | $n = 2000$ | |
	mean	max	mean	max	mean	max
P.1	8	12	8	13	8	13
P.2	8	14	7.8	13	8	15
GIES	7960	14715	449	909	284	553

5.3   Protein Expression Data

We illustrate our algorithm on the well-known protein expression dataset from [43]. Similar to [55], we processed the dataset into one observational and five one-node interventional datasets with 5846 samples of 11 nodes in total. The CPDAG of the conventionally accepted model of the interactions between

nodes serves as ground truth; this consensus $\mathcal{I}$-CPDAG and the one estimated by our algorithm can be found in the Appendix. Table 2 shows the SHD to the consensus $\mathcal{I}$-CPDAG; the statistics for the other algorithms are taken from [6, Tab. 3]. Although the ground truth is a DAG with 18 edges, our algorithm's performance is comparable to that of more general methods.

Table 2: Structural Hamming Distance to the consensus $\mathcal{I}$-CPDAG of the protein network from [43].

	Method					
	P.1/P.2	GIES	IGSP	CAM	DCDI-G	DCDI-DSF
SHD	15	38	18	35	36	33

6 Conclusion

We proposed an approach to learn linear Gaussian polytree models from interventional data where the interventions have known targets. Our two-step approach of first learning the skeleton and then orienting the edges exploits the availability of interventional data at each step, all the while using only local computations with low-dimensional marginals. We emphasize that our methods are especially well suited for the high-dimensional setting, with large graphs but moderate sample size.

To conclude, we highlight topics that emerge as future directions.

Unknown interventions: A natural extension of our work is to allow for unknown intervention targets. Although the skeleton recovery and collider search procedures apply in this case, the remaining orientation subroutines do not because they operate by searching $\mathcal{I}$-identifiable edges; this, in turn, depends on the characterization of $\mathcal{I}$-Markov equivalence which requires explicit knowledge of $\mathcal{I}$. The notion of Ψ-Markov equivalence, introduced in Jaber et al. [28], for unknown intervention targets appears to be a reasonable candidate to replace the use of the $\mathcal{I}$-MEC. The reason being that the Ψ-Markov equivalence class (Ψ-Markov EC) is a generalization of the $\mathcal{I}$-MEC in this case [28, App. D].

Forests: We focused on connected polytrees, but a generalization to disconnected forests of polytrees would be of interest. Undirected forests have been studied by Edwards et al. [16], but their construction does not carry over naturally to the directed case, and new research is needed.

Hidden variables: The algorithms we propose do not address the case where some variables remain hidden. For purely observational data from a polytree model, the hidden variable setting was considered by Sepehr and Materassi [44]. These authors provide necessary and sufficient conditions for causal structure recovery of the polytree with hidden nodes. It would be interesting to investigate to what extent interventional data would improve the identifiability of the polytree structure when such conditions are not met. Similar to the unknown interventions case, a possible approach would be to replace the $\mathcal{I}$-MEC by the Ψ-Markov EC because its level of generality encompasses hidden variables also.

Acknowledgements

A Notes on Consistency

Notation and assumptions:

a) Let $\mathcal{G} = (V, E)$, with $|V| = p$, be the polytree that underlies the data-generating distribution. Let $\mathcal{S}$ be its skeleton, and let $\mathcal{I} = \{I_1, \ldots, I_k\}$ be a conservative set of intervention with Σ_I being the covariance matrix associated to interventional setting $I \in \mathcal{I}$. We write $\rho^I_{u,v}$ for the correlation

between X_u and X_v in the setting I. Finally, let $w = (w_1, \ldots, w_k) \in [0,1]^k$, $\sum_j w_j = 1$, be the vector giving the probabilities that the i-th sample is taken from the interventional setting I_j.

b) Following [25], we assume that we jointly sample the interventional setting I_i and $X_i^{I_i}$, and that

$$X_i^{I_i}|I_i \sim \mathcal{N}(0, \Sigma_{I_i}).$$

c) Let $X = (X_1^{I_1}, X_2^{I_2}, \ldots, X_n^{I_n}) \in \mathbb{R}^{p \times n}$ be our sample. We write $\rho_{u,v}^I$ and $\hat{\rho}_{u,v}^I$ for the population and the sample correlation between X_u^I and X_v^I. Here, the sample quantity is computed using $X^I = (X_{i_1}^I, \ldots, X_{i_{n_I}}^I)$, where $\{i_1, \ldots, i_{n_I}\}$ is the set of all indices j with $I_{i_j} = I$.

d) Let $\rho_m^I := \min_{u,v} |\rho_{u,v}^I|$ and $\rho_M^I := \max_{u,v} |\rho_{u,v}^I|$, where the min and max extend over pairs of nodes u, v that are joined by an edge in the polytree $\mathcal{G}$. We assume

$$0 < \rho_m^I < \rho_M^I < 1 \ \text{ for all } I \in \mathcal{I}.$$

e) Let $\gamma_I = \rho_m^I (1 - \rho_M^I)/2$.

A.1   Consistency of Skeleton Recovery

In this section we provide finite sample analysis and prove consistency for the skeleton recovery under the assumptions a)-e) laid above. The following lemma is a straightforward modification of Lou et al. [33, Thm. 3.4].

Lemma A.1. *If for all $u, v \in V$ and all $I \in \mathcal{I}$ we have*

$$|\hat{\rho}_{u,v}^I - \rho_{u,v}^I| \leq \gamma_I,$$

then the Chow-Liu algorithm computed with the weighted mean function outputs the correct skeleton of the tree.

Proposition A.2. *Let $\hat{\mathcal{S}}_n$ be the output of the Chow-Liu algorithm computed with the weighted mean function, on a sample of size n, then*

$$\mathbb{P}(\hat{\mathcal{S}}_n \neq \mathcal{S}) \leq C_1 \binom{p}{2}(n-2)\left[\exp(-n) + \sum_{I \in \mathcal{I}} \exp\left[-\left(1 - (4 - \frac{n}{\beta_I})/nw_I\right)^2 \frac{nw_I}{2}\right]\right]$$

$$+ C_1 \binom{p}{2}(n-2)\left[\sum_{I \in \mathcal{I}} \exp\left[-\left(1 - 4/nw_I\right)^2 \frac{nw_I}{2}\right]\right],$$

where C_1 is a positive constant and $\beta_I = \log \frac{4 - \gamma_I^2}{4 + \gamma_I^2} < 0$.

Proof. From Lemma A.1, we have

$$\mathbb{P}(\hat{\mathcal{S}}_n = \mathcal{S}) \geq \mathbb{P}(\bigcap_{\substack{u,v \in V \\ I \in \mathcal{I}}} \{|\rho_{u,v}^{\hat{I}} - \rho_{u,v}^I| \leq \gamma_I\}) = 1 - \mathbb{P}(\bigcup_{\substack{u,v \in V \\ I \in \mathcal{I}}} \{|\hat{\rho}_{u,v}^I - \rho_{u,v}^I| > \gamma_I\}).$$

Now, we prove that this lower bound converges to 1 as $n \to \infty$ by showing that

$$\mathbb{P}(\bigcup_{\substack{u,v \in V \\ I \in \mathcal{I}}} \{|\hat{\rho}_{u,v}^I - \rho_{u,v}^I| > \gamma_I\}) \xrightarrow{n \to \infty} 0.$$

Indeed, by conditioning on the size $(n_1, \ldots, n_k)$ of the interventional data sets, we can write

$$\mathbb{P}(\bigcup_{\substack{u,v \in V \\ I \in \mathcal{I}}} \{|\hat{\rho}_{u,v}^I - \rho_{u,v}^I| > \gamma_I\}) = \sum_{\mathbf{n} = (n_1, \ldots, n_k)} \mathbb{P}\left(\bigcup_{\substack{u,v \in V \\ I \in \mathcal{I}}} \{|\hat{\rho}_{u,v}^I - \rho_{u,v}^I| > \gamma_I\} \mid \mathbf{n}\right) \mathbb{P}(\mathbf{n}).$$

14

Applying a union bound, we get

$$\mathbb{P}\Big(\bigcup_{\substack{u,v\in V \\ I\in\mathcal{I}}} \{|\hat{\rho}_{u,v}^I - \rho_{u,v}^I| > \gamma_I\}\Big) \leq \sum_{u,v\in V, u\neq v} \sum_{\mathbf{n}=(n_1,\ldots,n_k)} \mathbb{P}\Big(\bigcup_{I\in\mathcal{I}}\{|\hat{\rho}_{u,v}^I - \rho_{u,v}^I| > \gamma_I\} \mid \mathbf{n}\Big)\mathbb{P}(\mathbf{n}).$$

Using Kalisch and Bühlmann [30, Lemma 1], the conditional probabilities can be upper bounded as

$$\sum_{\mathbf{n}=(n_1,\ldots,n_k)} \mathbb{P}\Big(\bigcup_{I\in\mathcal{I}}\{|\hat{\rho}_{u,v}^I - \rho_{u,v}^I| > \gamma_I\} \mid \mathbf{n}\Big)\mathbb{P}(\mathbf{n})$$

$$\leq C \sum_{\substack{\mathbf{n}=(n_1,\ldots,n_k) \\ n_I>4,\forall I\in\mathcal{I}}} \sum_{I\in\mathcal{I}} (n_I - 2)\exp\Big((n_I - 4)\beta_I\Big)\mathbb{P}(\mathbf{n}) + c\mathbb{P}(\exists I \mid n_I \leq 4)$$

$$\leq C(n-2) \sum_{\substack{\mathbf{n}=(n_1,\ldots,n_k) \\ n_I>4,\forall I\in\mathcal{I}}} \sum_{I\in\mathcal{I}} \exp\Big((n_I - 4)\beta_I\Big)\mathbb{P}(\mathbf{n}) + c\mathbb{P}(\exists I \mid n_I \leq 4)$$

for some positive constants c, C and the negative coefficient

$$\beta_I = \log\frac{4 - \gamma_I^2}{4 + \gamma_I^2}.$$

For all $\delta > 0$, define
$$A_\delta = \{(n_1,\ldots,n_k) : \exp((n_I - 4)\beta_I) < \delta, \forall I \in \mathcal{I}\},$$

and let $B_\delta = A_\delta^c$ be its complement. Then we may bound our probability of interest as

$$\mathbb{P}\Big(\bigcup_{\substack{u,v\in V \\ I\in\mathcal{I}}} \{|\hat{\rho}_{u,v}^I - \rho_{u,v}^I| > \gamma_I\}\Big) \leq \binom{p}{2}(n-2)\Big[\sum_{\substack{(n_1,\ldots,n_k) \\ n_I>4,\forall I\in\mathcal{I}}} \sum_{I\in\mathcal{I}} \exp\Big((n_I - 4)\beta_I\Big)\mathbb{P}(\mathbf{n}) + c\mathbb{P}(\exists I \mid n_I \leq 4)\Big]$$

that is upper bounded by

$$C_1\binom{p}{2}(n-2)\Big[(\delta\mathbb{P}(A_\delta) + \mathbb{P}(B_\delta)) + c\mathbb{P}(\exists I \mid n_I \leq 4)\Big] \leq C_1\binom{p}{2}(n-2)\Big[(\delta + \mathbb{P}(B_\delta)) + c\mathbb{P}(\exists I \mid n_I \leq 4)\Big]$$

for some positive constant C_1, where in the last inequality we only used $\mathbb{P}(A_\delta) \leq 1$.

In order to do so, we rewrite

$$B_\delta = \{(n_1,\ldots,n_k) \mid \exists I \in \mathcal{I}, n_I < 4 + \log(\delta)/\beta_I\}$$
$$= \bigcup_{I\in\mathcal{I}} \{n_I < 4 + \log(\delta)/\beta_I\}.$$

Since $n_I \sim \text{Bin}(n, w_I)$, using Chernoff's bound we find that

$$\mathbb{P}(B_\delta) \leq \sum_{I\in\mathcal{I}} \exp\Big[-\Big(1 - (4 + \frac{\log(\delta)}{\beta_I})/nw_I\Big)^2 \frac{nw_I}{2}\Big]. \tag{11}$$

Using $\delta = \exp(-n)$ we get the following bound:

$$\mathbb{P}(\hat{\mathcal{S}}_n \neq \mathcal{S}) \leq C_1\binom{p}{2}(n-2)\Big[\exp(-n) + \sum_{I\in\mathcal{I}} \exp\Big[-\Big(1 - (4 - \frac{n}{\beta_I})/nw_I\Big)^2 \frac{nw_I}{2}\Big]\Big]$$
$$+ C_1\binom{p}{2}(n-2)\sum_{I\in\mathcal{I}} \exp\Big[-\Big(1 - 4/nw_I\Big)^2 \frac{nw_I}{2}\Big], \tag{12}$$

where we bounded $\mathbb{P}(\exists I \mid n_I \leq 4)$ with the same Chernoff bound we used in Eq. (11). $\qquad\square$

Proposition A.3. *Assume that the number of experiments $|\mathcal{I}|$ does not depend on n, and that there are constants $\gamma_*, w_* > 0$ such that $\min_{I \in \mathcal{I}} \gamma_I > \gamma_*$ and $\min_{I \in \mathcal{I}} w_I > w_*$ uniformly in n. If $\log p = o(n)$, then*

$$\mathbb{P}(\hat{\mathcal{S}}_n \neq \mathcal{S}) \xrightarrow{n \to \infty} 0.$$

Proof. Let $\beta_* = \log \frac{4 - \gamma_*^2}{4 + \gamma_*^2} < 0$. Then $\beta_I < \beta_* < 0$ for all $I \in \mathcal{I}$. Thus, there is a constant $C' \equiv C'(\beta_*, w_*) > 0$ such that for all large n, all terms on the right-hand side of Eq. (12) are bounded from above by

$$C_1 p^2 n \exp\left[-C' \frac{n w_*}{2} \right] < C_1 p^2 \exp\left[-C_2 n \right]$$

for a further smaller constant $C_2 = C_2(\beta_*, w_*)$. Hence the consistency claim holds under the assumption that $\log p = o(n)$. $\qquad\square$

A.2 Consistency of Orientation Procedures

A finite-sample analysis of the orientation procedures is more subtle, and what we present below is instead a discussion of consistency in the setting of growing sample size but fixed dimension. The difficulties in a more refined analysis lie primarily with the BIC-based procedure as it involves tests based on likelihood ratios that are obtained by optimizing a generally nonconvex function. For the IRC procedure, a high-dimensional analysis could be performed using concentration inequalities for non-central chi-square distributions [21].

A.2.1 BIC

In [25], it is proven that under the assumptions a)-e) stated at the beginning of this section of the supplement the model can be parametrized as an exponential family, so the consistency for the orientation part follows from classical consistency results on the BIC criterion for exponential families, see e.g. Drton et al. [15, Thm. 5.13].

Proposition A.4. *Let $u \to v \in G$ be directly G-identifiable, and let $\mathcal{H}_{u \to v}, \mathcal{H}_{u \leftarrow v}$ be the correctly specified models in which we allow the variance to vary only if there is a possible ancestor of the node that has been intervened upon, while $\tilde{\mathcal{H}}_{u \to v}$ and $\tilde{\mathcal{H}}_{u \leftarrow v}$ are the models in which we relax the variance constraints and let them vary also in the environments in which there are no ancestors that have been intervened upon. Then under generic data-generating distributions in $\mathcal{H}_{u \to v}$ we have:*

$$\mathbb{P}(l_{\tilde{\mathcal{H}}_{u \to v}} > l_{\tilde{\mathcal{H}}_{u \leftarrow v}}) \xrightarrow{n \to \infty} 0.$$

Proof. Consider first the case in which there is an $I_0 \in \mathcal{I}$ such that $I_0 \cap \{u, v\} = \{u\}$. In this case, it holds that $\mathbb{P}(l_{\tilde{\mathcal{H}}_{u \to v}} > l_{\tilde{\mathcal{H}}_{u \leftarrow v}}) \xrightarrow{n \to \infty} 0$ provided the true data-generating distribution belongs to $\mathcal{H}_{u \to v}$ but not the relaxed alternative $\tilde{\mathcal{H}}_{v \to u}$. We now claim that the intersection $\mathcal{H}_{u \to v} \cap \tilde{\mathcal{H}}_{v \to u}$ corresponds to a measure zero subset of $\mathcal{H}_{u \to v}$. To see this note that even in the larger model $\tilde{\mathcal{H}}_{v \to u}$ we have $\lambda_{v \to u}^{\emptyset} = \lambda_{v \to u}^{I_0}$, where the involved quantities can be written as rational functions of the model parameters:

$$\lambda_{v \to u}^I = \frac{\lambda_{u \to v}^I \sigma_u^I}{(\lambda_{u \to v}^I)^2 \sigma_u^I + \sigma_{v|u}^I}, \qquad I = \emptyset, I_0.$$

Hence, imposing the condition $\lambda_{v \to u}^{\emptyset} = \lambda_{v \to u}^{I_0}$ amounts to a *non-trivial* rational equation also on $\mathcal{H}_{u \to v}$, which implies that $\mathcal{H}_{u \to v} \cap \tilde{\mathcal{H}}_{v \to u}$ is indeed a measure zero set in $\mathcal{H}_{u \to v}$.

We turn to the second case, where there is no set $I_0 \in \mathcal{I}$ with $I_0 \cap \{u, v\} = \{u\}$. Since we assume the orientation of the edge $\{u, v\}$ to be $\mathcal{I}$-directly-identifiable, there has to be at least one I_1 such that $I_1 \cap \{u, v\} = \{v\}$. This implies that the dimension of $\tilde{\mathcal{H}}_{u \to v}$ is smaller than that of $\tilde{\mathcal{H}}_{v \to u}$, so in the event in which the true parameters lie in $\mathcal{H}_{u \to v} \cap \tilde{\mathcal{H}}_{v \to u} \subseteq \tilde{\mathcal{H}}_{u \to v} \cap \tilde{\mathcal{H}}_{v \to u}$, the BIC will asymptotically select the model of lower dimension with probability converging to 1, which we have proven to be $\tilde{\mathcal{H}}_{u \to v}$. $\quad\square$
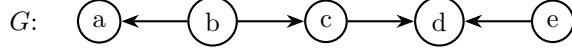
G: a ← b → c → d ← e

Figure B.1: Example B.1 describes the procedures P. 1 and P. 2 to learn the DAG G above with $\mathcal{I} = \{I_1 = \emptyset, I_2 = \{b\}\}$. The combination $(G, \mathcal{I})$ is such that every edge in G is $\mathcal{I}$-directly-identifiable.

Algorithm 1: FINDTHEROOT$(\mathcal{I}, X, N, \mathcal{G})$

Data: A set of intervention targets $\mathcal{I}$, a list of datasets X, a list of sample sizes N, an undirected graph $\mathcal{G}$.

Result: A directed tree $\mathcal{G}_d$

1 $\mathcal{G} = (V, E)$
2 $L \leftarrow 0$ vector of length $|V|$
3 **for** $v \in V$ **do**
4 $\quad | \quad L(v) \leftarrow$ Likelihood of the model in which v is the root
5 **end**
6 $r \leftarrow \arg\max L$
7 $\mathcal{G}_d \leftarrow$ directed tree with skeleton $\mathcal{G}$ and root node r

---

A.2.2 Invariance of Regression Coefficients (IRC)

Orientating edges using the IRC treats each $\mathcal{I}$ directly identifiable edge individually. Let $n = n_{I_0} + n_I$ be the total sample size to perform the test in Section IV-A of the main text. To justify the consistency of this test, note that as $n \to \infty$ it is possible to choose a sequence of significance levels α_n that decreases to zero suitably slowly, in such a way that the probability of a type I or a type II error both tend to zero. In practice, we treat the significance level as a tuning parameter of the algorithm.

B Orientation Procedures: Example and Pseudocode

The next example demonstrates each one of the procedures for a DAG on five nodes and a collection of intervention targets. Following the example, we provide pseudocode to perform each of the procedures outlined in Section IV.C and Section IV.D of the main text. These procedures rely on several subroutines, these are presented first in Algorithms 3,2, and 1. Immediately after we present the pseudocode for the procedures P. 1, P. 2 in Algorithms 4, 5.

Example B.1. *Here we show how to learn the graph in the Fig. B.1 where $\mathcal{I} = \{I_1 = \emptyset, I_2 = \{b\}\}$ and the skeleton of the graph is already known.*

(i) Procedure 1 would first test $X_a \perp\!\!\!\perp X_c, X_b \perp\!\!\!\perp X_d$ and $X_c \perp\!\!\!\perp X_e$, finding that only the last triplet forms a collider and so orienting $c \to d \leftarrow e$. After this step, to orient the subtree $a - b - c$ Procedure 1 would either compute the BIC scores of the three models $\mathcal{M}_a = a \to b \to c$, $\mathcal{M}_b = a \leftarrow b \to c$ and $\mathcal{M}_c = a \leftarrow b \leftarrow c$, finding that b is the root, or would use the test for the invariance of the regression coefficients for $a - b$ and $b - c$ orienting the two edges independently.

(ii) Procedure 2 would orient the edges $a \leftarrow b$ and $b \to c$ using using either the BIC score or the IRC test. Then, it would orient the edge $c \to d$ testing $X_b \perp\!\!\!\perp X_d$ and finally orient $d \leftarrow e$ testing $X_c \perp\!\!\!\perp X_e$.

Algorithm 2: COLLIDER($I, X, N, E, O, COLL$)

Data: A set of intervention targets $\mathcal{I}$, a list of datasets X, a list of sample sizes N, a list of unoriented edges E, a list of oriented edges O, an indicator $COLL$ indicates the BIC score to use for the collider search when one edge has already been oriented.

Result: An augmented list of oriented edges O, a list of unoriented edges E

```
1  while F == TRUE do
2  │   F ← TRUE
3  │   for u → v ∈ O do
4  │   │   for v − w ∈ E do
5  │   │   │   if X_u^I ⫫ X_w^I, ∀I ∈ I;                    /* using COLL */
6  │   │   │   then
7  │   │   │   │   E ← E \ {v − w}
8  │   │   │   │   O ← O ∪ {w → v}
9  │   │   │   │   F ← FALSE
10 │   │   │   else
11 │   │   │   │   E ← E \ {v − w}
12 │   │   │   │   O ← O ∪ {v → w}
13 │   │   │   │   F ← FALSE
14 │   │   │   end
15 │   │   end
16 │   end
17 │   for u − v − w ∈ E do
18 │   │   if X_u^I ⫫ X_w^I, ∀I ∈ I then
19 │   │   │   E ← E \ {{u, v}, {v, w}}
20 │   │   │   O ← O ∪ {u → v, w → v}
21 │   │   │   F ← FALSE
22 │   │   end
23 │   end
24 end
```

Algorithm 3: RECURSIVE COLLIDER
($\mathcal{I}, X, N, E, O, o$)

Data: A set of intervention targets $\mathcal{I}$, a list of datasets X, a list of sample sizes N, a list of unoriented edges E, a list of oriented edges O, an oriented edge $o = (u \to v)$, an indicator $COLL$ indicating the BIC score to use for the collider search when one edge has already been oriented.

Result: A list of oriented edges O, a list of unoriented edges E

```
1  for (v, w) ∈ E do
2  │   if X_u^I ⫫ X_w^I, ∀I ∈ I;                           /* using COLL */
3  │   then
4  │   │   E ← E \ {v, w}
5  │   │   O ← O ∪ {v ← w}
6  │   else
7  │   │   E ← E \ {v, w}
8  │   │   O ← O ∪ {v → w}
9  │   │   E, O ← RECURSIVE COLLIDER (I, X, N, E, O, o = (v → w), COLL)
10 │   end
11 end
```

Algorithm 4: Procedure 1

$(\mathcal{I}, X, N, V, E, PW, COLL)$

Data: A set of intervention targets $\mathcal{I}$, a list of datasets X, a list of sample sizes N, a list of vertices V, a list of undirected edges E, an indicator PW that indicates if using the BIC scores or the test of the invariance of the regression coefficients, an indicator $COLL$ indicates the BIC score to use for the collider search when one edge has already been oriented.

Result: Interventional CPDAG $\mathcal{G}$

1 $E, O \leftarrow$ COLLIDER $(\mathcal{I}, X, N, E, O = \emptyset, COLL)$

2 $\mathcal{G} \leftarrow (V, O)$

3 **if** $PW ==$"BIC" **then**

4 $\quad$ $\mathcal{G} \leftarrow (V, E)$

5 $\quad$ $\mathcal{G}_1, \ldots, \mathcal{G}_k \leftarrow$ connected components of $\mathcal{G}$

6 $\quad$ **for** $i \in \{1, \ldots, k\}$ **do**

7 $\quad\quad$ $\mathcal{G}_d \leftarrow$ FINDTHEROOT $(\mathcal{G}_i)$

8 $\quad\quad$ $\mathcal{G} \leftarrow \mathcal{G} \cup \mathcal{G}_d$

9 $\quad$ **end**

10 $\quad$ $\mathcal{G} \leftarrow \mathcal{I}$-CPDAG$(\mathcal{G})$

11 **else**

12 $\quad$ **for** $e \in E$ **do**

13 $\quad\quad$ **if** e *is directly* $\mathcal{I}$ *identifiable* **then**

14 $\quad\quad\quad$ $o \leftarrow$ directed version of e ; $\quad\quad\quad\quad\quad\quad\quad\quad\quad$ /* using PW */

15 $\quad\quad\quad$ $E, O \leftarrow$ RECURSIVE COLLIDER $(\mathcal{I}, X, N, E, O, o, COLL)$

16 $\quad\quad$ **end**

17 $\quad$ **end**

18 $\quad$ $\mathcal{G} \leftarrow (V, (E \cup O))$

19 **end**

Algorithm 5: Procedure 2

$(\mathcal{I}, X, N, V, E, PW, COLL)$

Data: A set of intervention targets $\mathcal{I}$, a list of datasets X, a list of sample sizes N, a list of vertices V, a list of undirected edges E, an indicator PW that indicated if using the BIC scores or the test of the invariance of the regression coefficients, an indicator $COLL$ indicated the BIC score to use for the collider search when one edge has already been oriented.

Result: Interventional CPDAG $\mathcal{G}$

1 $O \leftarrow \emptyset$

2 **for** $e \in E$ **do**

3 $\quad$ **if** e *is directly* $\mathcal{I}$ *identifiable* **then**

4 $\quad\quad$ $o \leftarrow$ directed version of e ; $\quad\quad\quad\quad\quad\quad\quad\quad\quad$ /* using PW */

5 $\quad\quad$ $E \leftarrow E \setminus \{e\}$

6 $\quad\quad$ $O \leftarrow O \cup \{o\}$

7 $\quad$ **end**

8 **end**

9 $E, O \leftarrow$ COLLIDER$(\mathcal{I}, X, N, E, O, COLL)$

10 $\mathcal{G} \leftarrow (V, (E \cup O))$

C Extended Simulation Studies

In this section we present further analysis of the behaviour of our algorithms.

C.1 Description of Computational Settings

When the generated graph is a polytree we first sample a random undirected trees by generating random Prfer sequences [40] and then independently orienting each edge, while the DAGs are generated either via Erdős-Rényi or Barabasi-Albert model [3, Chap. III,VII]. For the coefficient matrices Λ, we draw each coefficient uniformly in $(-2, -0.5) \cup (0.5, 2)$. To obtain samples, we multiply a Gaussian error vector with the matrix $(I - \Lambda)^{-T}$, the variances of the error vector are sampled uniformly in $[0.05, 0.15]$. To ease the comparison with the algorithm, we use the same setup for simulate intervention that is used in [19]. Each intervention changes the mean of the intervened variable in the following way: First a parameter $\hat{\mu}_{k,i}$ is sampled from $\mathcal{N}(0, 2)$, then the interventional mean is set to $\mu_{k,i}^I = 5 \cdot \mathrm{sign}(\hat{\mu}_{k,i}) + \hat{\mu}_{k,i}$. The interventional variance is set to 0.5 for all the intervened nodes. Other types of interventions behave similarly and can be seen in Section C.4. The performance of our learning procedures is measured by the structural Hamming distance (SHD) adapted to CPDAGs from [24]. All code is available at [53].

For all simulations, except the ones for Fig. 1c (left) in the main paper and Section C.6, the sample size of all interventional and observational data sets is $n/|\mathcal{I}|$ where n is the total sample size. For settings where the size of the interventions is one ($k = 1$), the intervention targets of all data sets are always different. If $k > 1$, this is also the case, although it is possible that two different sets of intervention targets intersect nontrivially.

The baseline of the skeleton recovery, denoted baseObs in Fig. 1 of the main text, corresponds to the Chow-Liu algorithm executed on the weight matrix of only the observational data. The low-dimensional setting in Fig. 3 of the main text is 20 nodes and all one-node intervention targets. The high-dimensional setting in Fig. 3 of the main text is 500 nodes with 10 interventional datasets that each intervene on 10 randomly chosen nodes. Each simulation was repeated 20 times in the low dimensional case and 10 times in the high-dimensional case.

C.2 Skeleton recovery

Pooled data: Fig. C.1 shows the performance of the three skeleton recovery procedures against two baselines; "pooled" that is computed using the Chow-Liu algorithm with the correlation matrix of the pooled data, and "baseObs" that is computed using observational data only. The "Flipped" intervention changes the sign of the regression coefficient. We observe that, when doing perfect interventions or interventions where the sign of the coefficients doesn't change, "pooled" exhibits superior performance than the methods using the aggregation functions. Pooling the data does not perform well when the intervention changes the sign of the coefficients, especially when the number of intervened nodes is high, this shows that the correlation matrix of the pooled data doesn't give rise to a G-valid matrix.

Running times: Fig. C.2 shows the runtime of the skeleton recovery procedures in the high-dimensional setting ($p = 500, n = 1000$). The parameters in this figure are similar to those in Fig. 1 of the main text. As expected, mean and Itest are substantially faster than median since they only require arithmetic operations.

C.3 Analysis of Orientation Recovery

In this section we analyze the performance of the different orientation procedures P. 1 and P. 2. For each procedure we have two choices: pairwise orientation with either BIC (Section 4.3.2 of the main text) or IRC (Section 4.3.1 of the main text) and finding the colliders with either simple (Section 4.4.1 of the main text) or refined (Section 4.4.2 of the main text). We analyze the performance of all eight possible procedures in Fig. C.3, where the four green scale colors indicate the four possibilities for P. 1 and the four blue scale colors indicate the four possibilities for P. 2.

In all simulations we use the true underlying skeleton of the polytree. As a comparison we record the mean SHD between the $\mathcal{I}$-CPDAG of the true polytree and a polytree obtained by randomly orienting each edge of the true skeleton. The plots in Fig. C.3 show the behaviour of the orientation procedures in
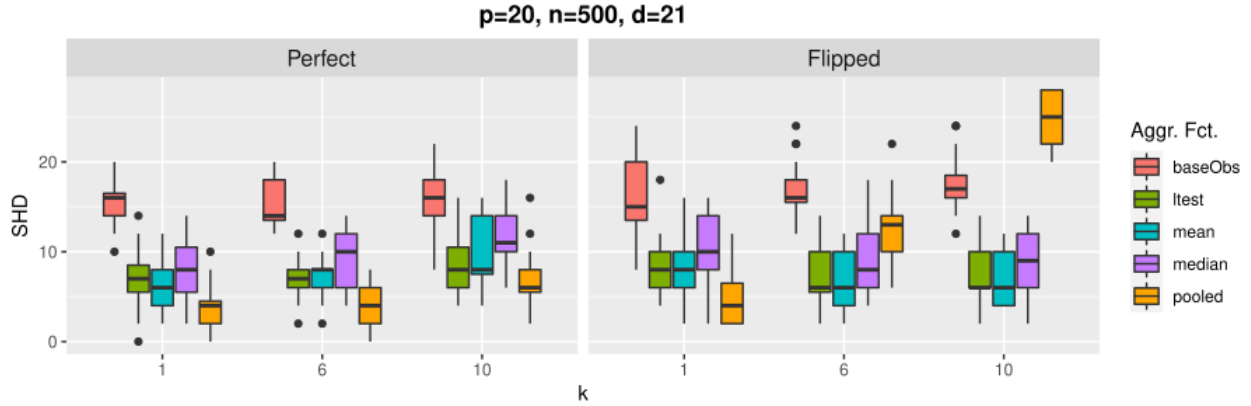
Figure C.1: Skeleton recovery with perfect interventions (left) and interventions where the sign of the coefficient is flipped (right).
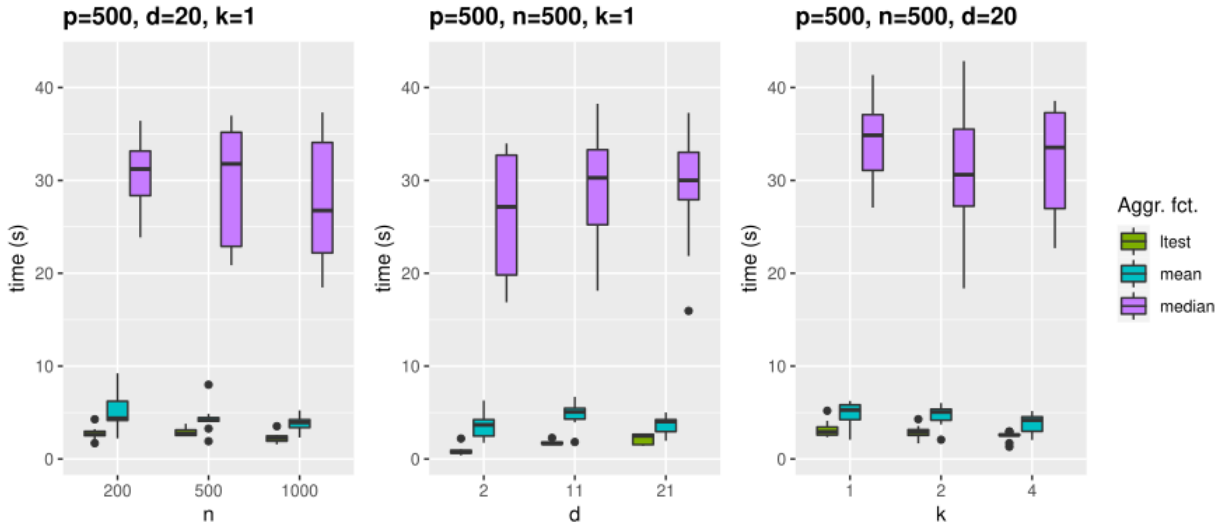

Figure C.2: Skeleton recovery with base parameters 500 nodes, 1000 samples and 20 intervention targets with 10 intervened nodes each. The labels Itest, mean, median indicate each of the procedures in the list in respectively.

low- and high- dimensional settings for varying parameters p =number of nodes, n = number of samples, d = number of data sets (i.e. number of interventional datasets plus the observational dataset), and k =number of nodes in each intervention. All plots in Fig. C.3 are for perfect interventions, other types of interventions behave similarly (see Section C.4 and Fig. C.5).

With an overall glance at Fig. C.3, it seems like P. 2 (blue) behaves better than P. 1 (green). This is especially the case for increasing number of intervened nodes (k), c.f. plots (c) and (d). This can be explained since more causal information can be recovered by targeting more nodes in each intervention. Nevertheless, P.1 behaves comparably in settings with few interventions and thus should be further considered. Increasing the number of datasets (d), however, does increase SHD, c.f. plot (e) and (f). This could be explained by the observation that increasing the number of data sets for a fixed total sample size decreases the sample size of each individual data set which can lead to more inaccurate results. Comparing refined and simple collider recovery, we notice that they have similar SHD, however, the simple methods are substantially faster, c.f. plots (g) and (h). Finally, we see that BIC has in general less SHD but is also substantially slower.

Overall, it seems most reasonable to compare both P.1 and P.2 equipped with simple collider search

and single edge orientation with IRC to guarantee accuracy as well as computational efficiency in high-dimensional settings.

C.4 Comparison with Other Types of Interventions (Orientation and Skeleton)

In this section we compare the behaviour of our algorithms under different types of interventions, namely: "Inhibitory" that sets the regression coefficient λ to 0.1λ and "Flipped" defined as in Section C.2.

Skeleton recovery. From Fig. C.4, we see that all the aggregation functions behave similarly under different intervention settings, except the pooling data under "Flipped" intervention that we already pointed out in Section C.2.

Orientation recovery: From the plots in Fig. C.5, we see that there is no difference between "Perfect" and "Inhibitory" intervention while for "Flipped" intervention P. 2 performs significantly better.
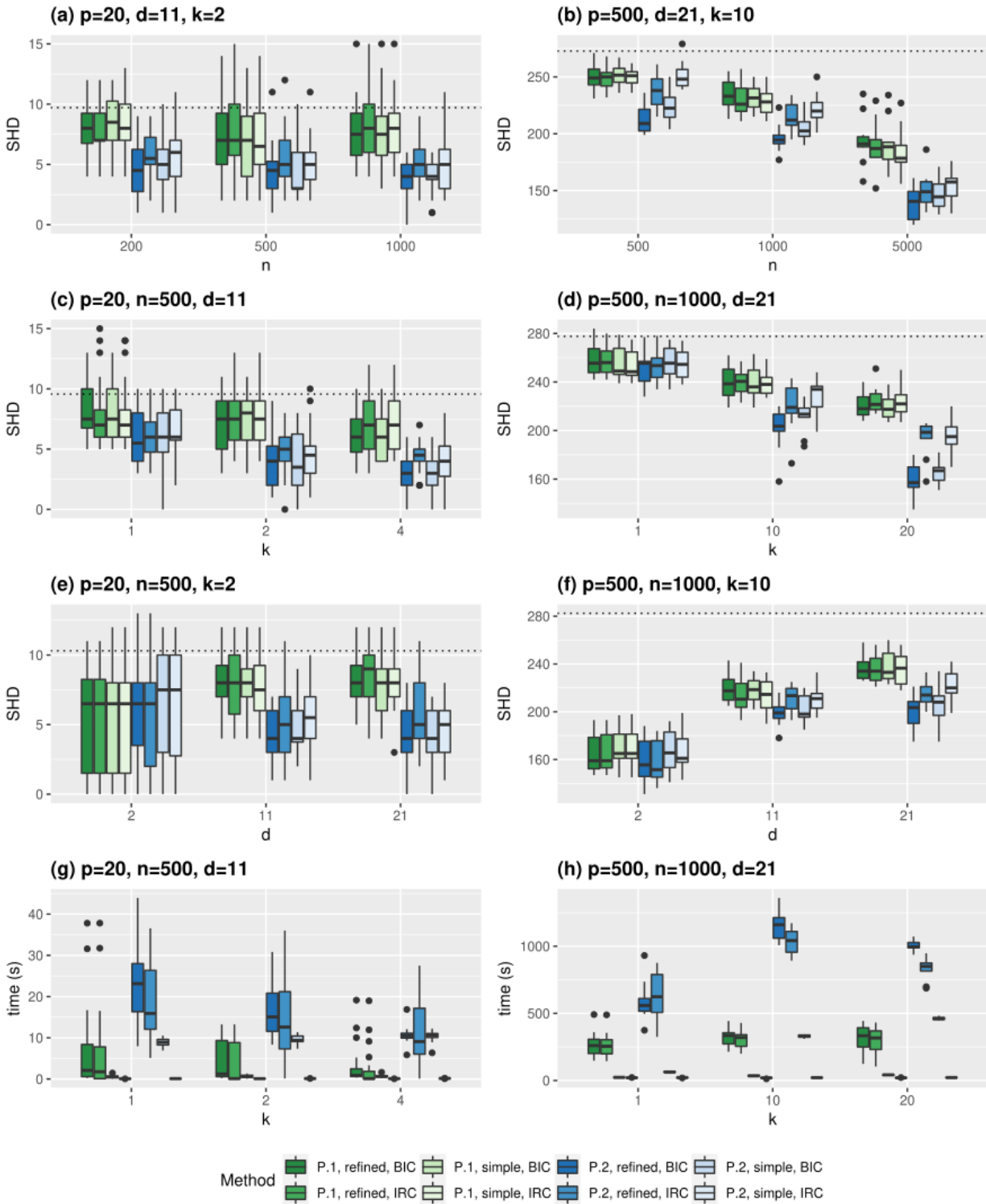
Figure C.3: Orientation recovery from true skeleton in low- (left column) and high-dimensional (right column) setting with varying parameters and base parameters given in the title of each plot. The dotted line denotes the baseline of randomly orienting the edges.
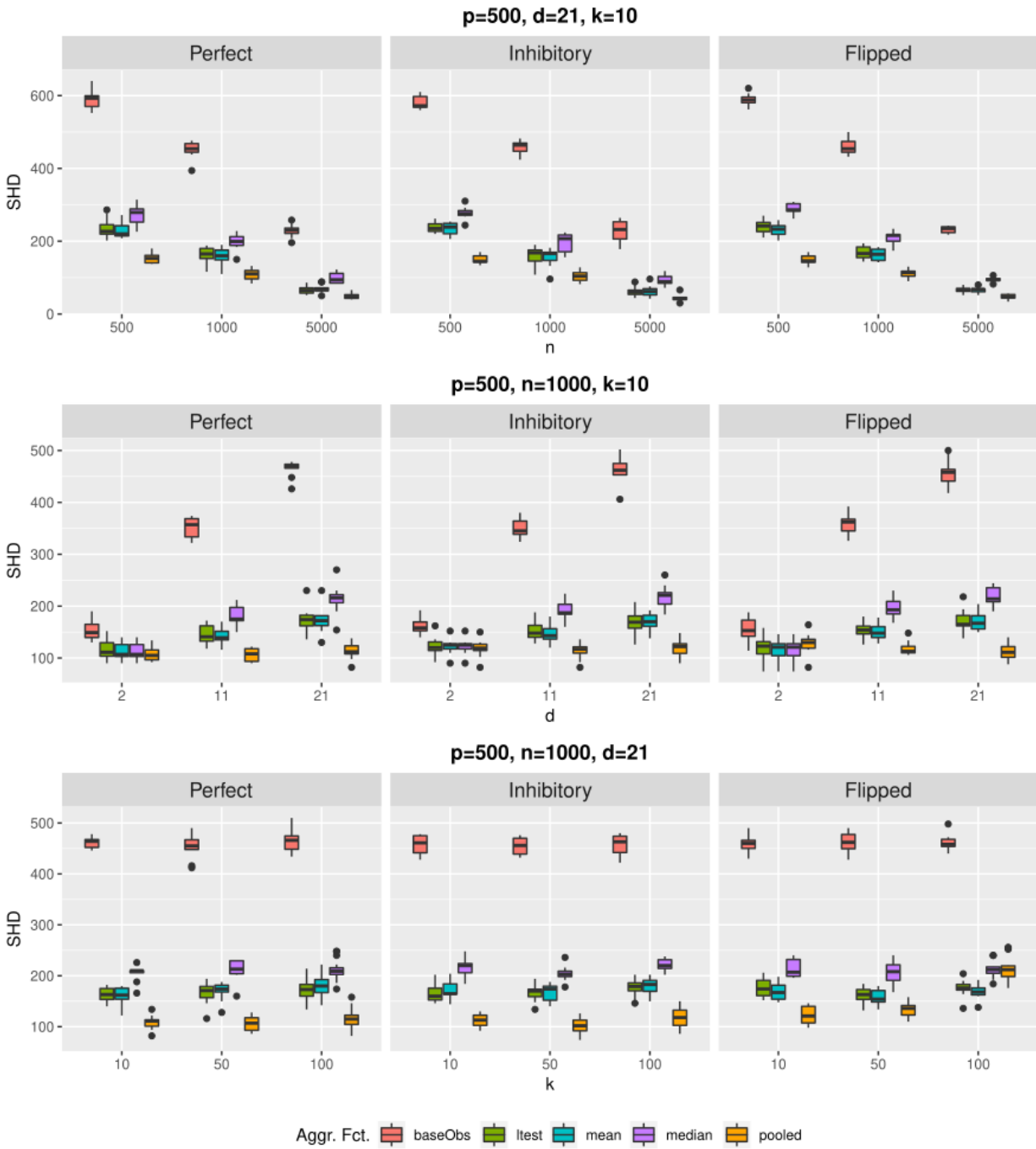
Figure C.4: Skeleton recovery with the intervention types perfect (left), inhibitory (middle) and flipped (right) in high-dimensional setting.
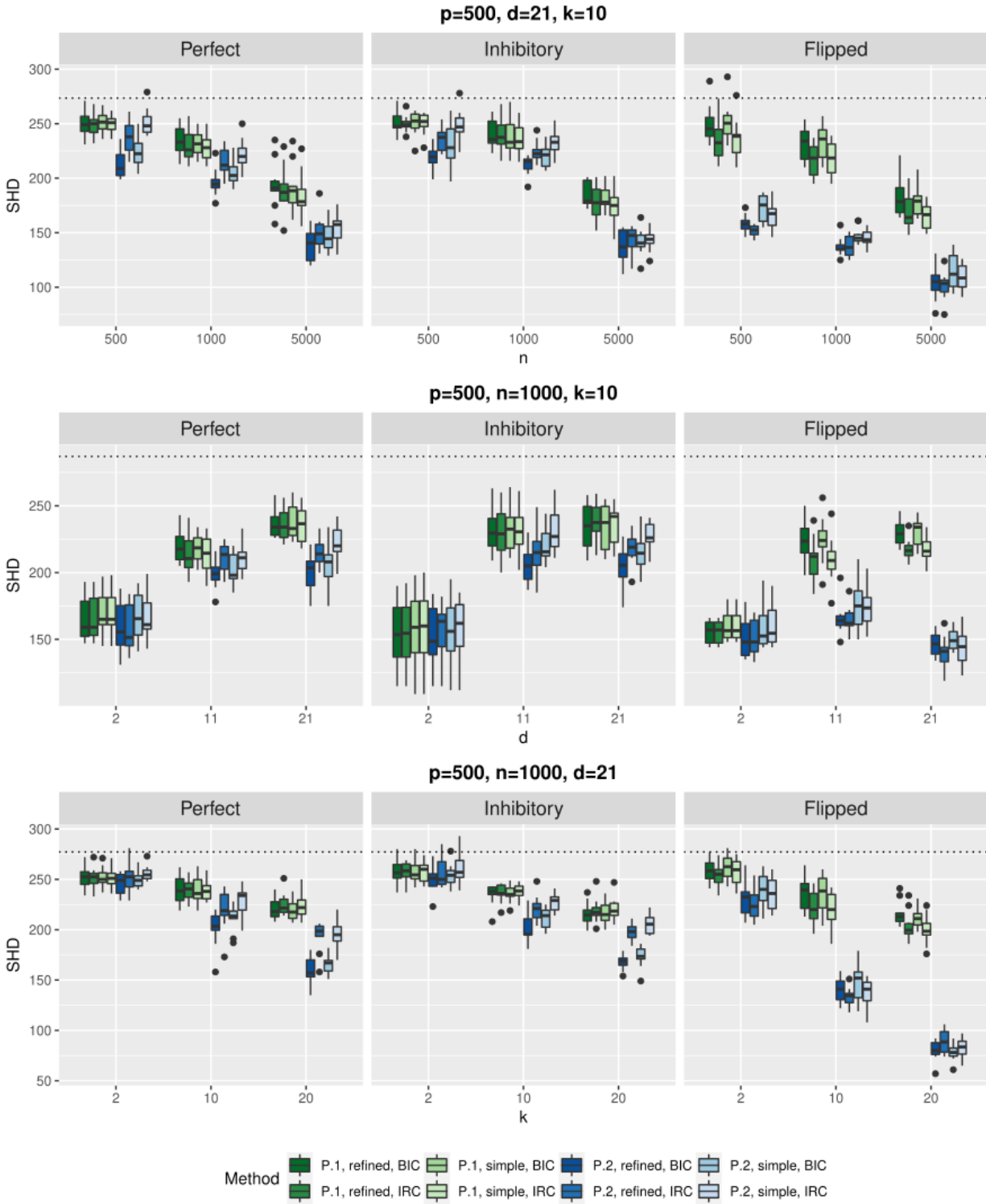
Figure C.5: Orientation recovery from true skeleton in high-dimensional settings under perfect (left), inhibitory (middle) and flipped (right) interventions. The dotted line denotes the baseline of randomly orienting edges.
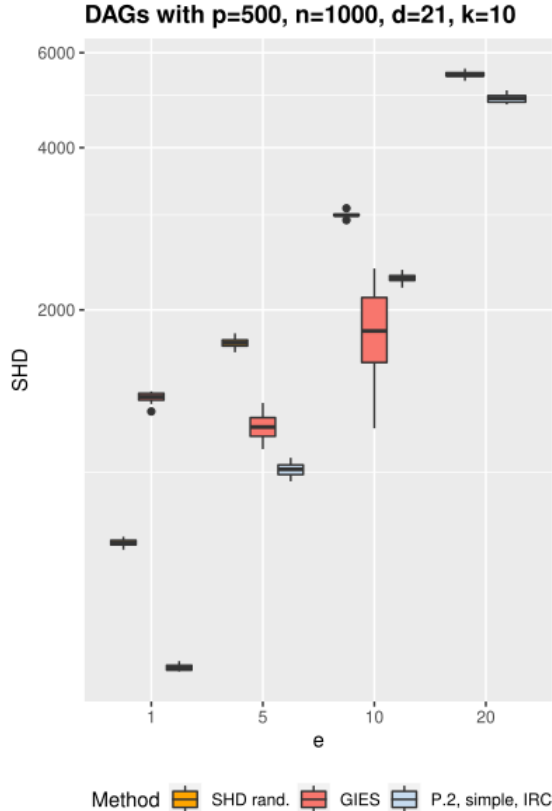
Figure C.6: Recovery of the $\mathcal{I}$-CPDAG of DAGs with varying expected number of edges per node e in high-dimensional setting. The box SHD rand. denotes the $\mathcal{I}$-CPDAG of randomly sampled polytrees. GIES on $e = 20$ could not be computed in less than 24h.

Table C.1: Mean and maximum runtime on DAGs with varying expected number of edges per node e using P. 2, simple, IRC.

| Method | Runtime in seconds | | | | | | | |
| | $e = 1$ | | $e = 5$ | | $e = 10$ | | $e = 20$ | |
	mean	max	mean	max	mean	max	mean	max
P. 2	7	9	7	9	8	10	8	11
GIES	129	143	220	249	865	1249	> 24h	> 24h

C.5 Further Comparisons with GIES

In Section V-B, Fig. 3 and Table I of the main text, we compared the performance of GIES with that of P. 1, simple, IRC and P. 2, simple, IRC. Here we expand this analysis by comparing GIES and P. 2 simple, IRC on DAGs with increasing expected number of edges per node, denoted by e. All the DAGs in the section are sampled from an Erdős-Rényi model. In terms of SHD, we see in Fig. C.6 that for $e = 1, 5$, P. 2, simple, IRC outperforms GIES. For increasing values of e it is expected that P. 2, simple, IRC will get worse in terms of SHD because the true underlying DAG is not a polytree. We see however that its performance is comparable that of GIES. The Table C.1 contains running times for these simulation. For $e = 1, 5$ P. 2, simple, IRC is faster than GIES by two orders of magnitude and three for $e = 10$, for $e = 20$ the GIES algorithm did not finish after 24hrs hence it was aborted.

Table C.2: Mean and maximum runtime on low dimensional DAGs

Method	Runtime in seconds	
	mean	max
IGSP	12.09	38.14
GIES	0.03	0.06
P.1, simple, BIC	0.32	0.91
P.1, simple, IRC	0.05	0.07
P.2, simple, BIC	6.01	7.69
P.2, simple, IRC	0.07	0.08
P.1, refined, BIC	8.40	81.23
P.1, refined, IRC	7.94	78.47
P.2, refined, BIC	12.37	26.79
P.2, refined, IRC	12.92	65.46
DCDI	18337.63	29762.54
dibs	1354.14	1372.32

C.6 Unbalanced Sample Sizes

Throughout the previous analyses, the sample size of each data set, both observational and interventional, are all equal. In this section we present simulations for the case when the observational data set has more samples than the interventional data sets. In particular, we denote with w_o the percentage of samples that are in the observational dataset, the samples that are not in the observational dataset are evenly distributed across the 20 interventional datasets. The scenario in which $w_o = 0.048$ correspond to a balanced sample.

Skeleton recovery: From the left plot in Fig. C.7, we see that the performance of Itest worsens when the data become more unbalanced, while the performance of median improves. Moreover, as predictable, we see that if the observational data is big enough the baseline that uses only observational data performs comparably with the other methods.

Orientation recovery: From the right plot in Fig. C.7 we see that P. 1 is unaffected from the unbalancing of the data, while the performances of P. 2 get slightly worse when the data are more unbalanced.

Comparison with GIES: From the plot in Fig. C.9 we see that the performance of GIES is negatively affected from unbalancing of the data, while the performance of our algorithm is overall unaffected. The simulations are performed with DAGs of size $p = 1000$ and expected number of edges per node $e = 5$.

C.7 Protein Expression Data

Table II in the main text shows the SHD between the consensus graph and the one produced by our algorithm. We show the two graphs in Fig. C.8.
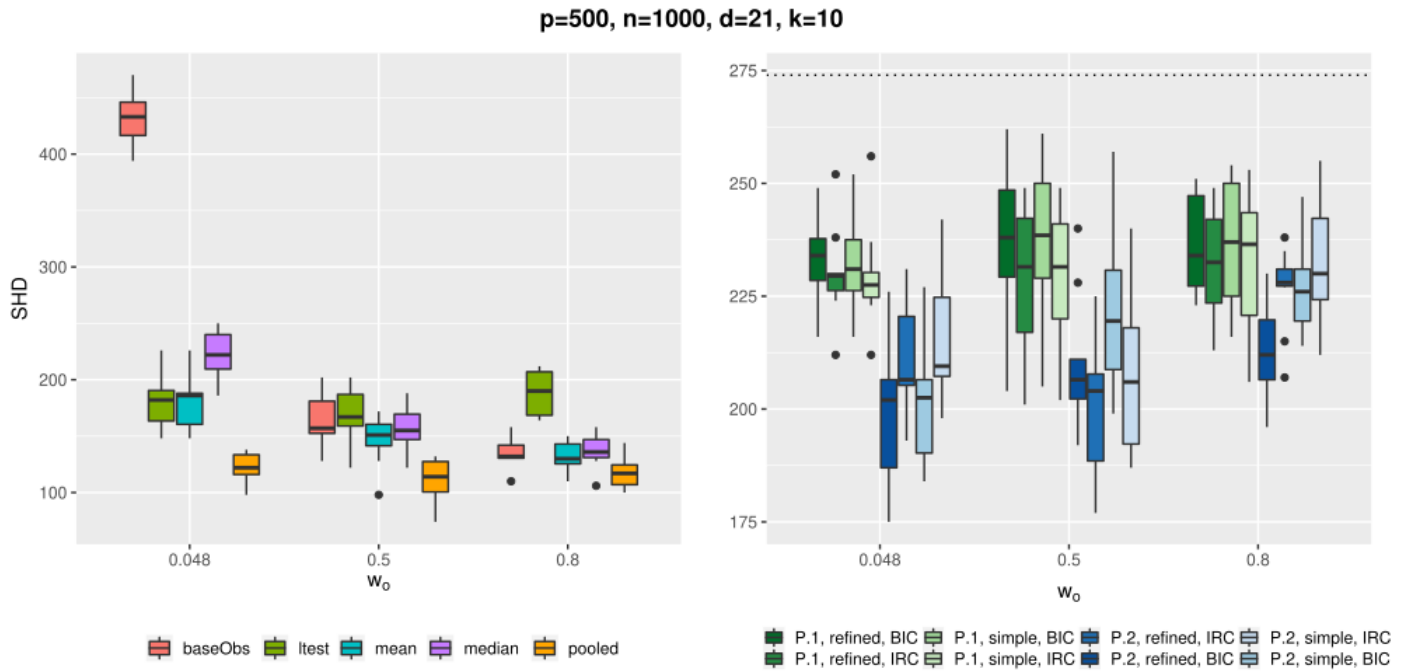
Figure C.7: Skeleton and orientation recovery with unbalanced sample sizes. The dotted line denotes the baseline of randomly orienting the edges. The value w_o is the percentage of samples that are in the observational dataset.
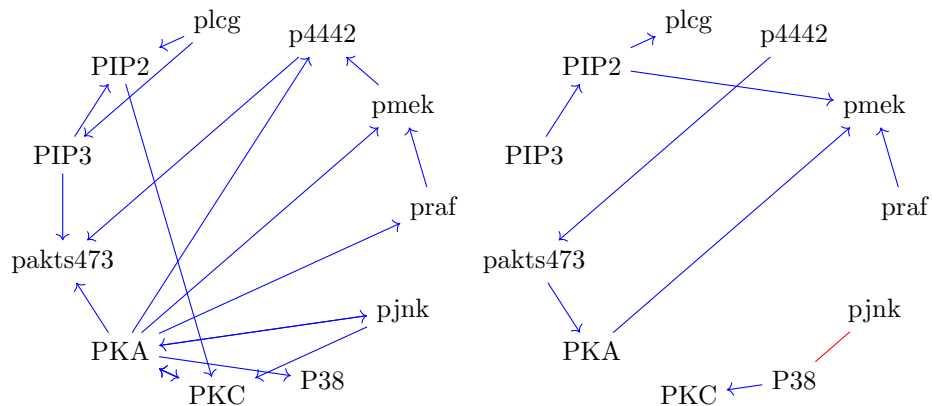

Figure C.8: On the top, the consensus I-CPDAG for the Sachs data, and on the bottom, the one estimated by our algorithm. Different versions of our algorithm output the same result in this case.
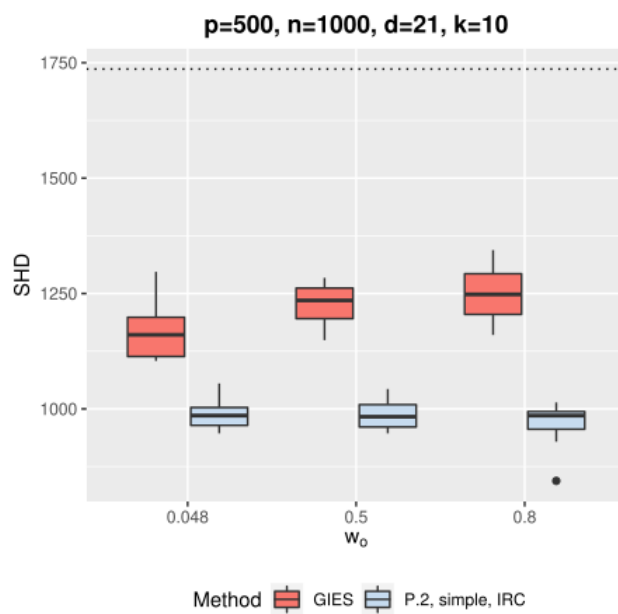
Figure C.9: Comparison between P. 2, simple, IRC and GIES on DAGS with expected number of edges per node $e = 5$. The dotted line denotes the baseline of randomly orienting the edges.

References

[1] Silvia Acid and Luis M. de Campos. Approximations of causal networks by polytrees: an empirical study. In *Advances in Intelligent Computing - IPMU'94, 5th International Conference on Processing and Management of Uncertainty in Knowledge-Based Systems*, volume 945 of *Lecture Notes in Computer Science*, pages 149–158. Springer, 1994.

[2] Sina Akbari, Ehsan Mokhtarian, AmirEmad Ghassami, and Negar Kiyavash. Recursive causal structure learning in the presence of latent variables and selection bias. *Advances in Neural Information Processing Systems*, 34:10119–10130, 2021.

[3] Réka Albert and Albert-László Barabási. Statistical mechanics of complex networks. *Rev. Mod. Phys.*, 74:47–97, Jan 2002.

[4] Carlos Amndola, Mathias Drton, Alexandros Grosdos, Roser Homs, and Elina Robeva. Third-order moment varieties of linear non-Gaussian graphical models. *Information and Inference: A Journal of the IMA*, 12(3):1405–1436, 2023.

[5] Mona Azadkia, Armeen Taeb, and Peter Bhlmann. A fast non-parametric approach for local causal structure learning. *arXiv:2111.14969*, 2021.

[6] Philippe Brouillard, Sébastien Lachapelle, Alexandre Lacoste, Simon Lacoste-Julien, and Alexandre Drouin. Differentiable causal discovery from interventional data. *Advances in Neural Information Processing Systems*, 33:21865–21877, 2020.

[7] K.P. Burnham and D.R. Anderson. *Model selection and multimodel inference: a practical information-theoretic approach*. Springer Verlag, 2002.

[8] Sourav Chatterjee and Mathukumalli Vidyasagar. Estimating large causal polytree skeletons from small samples. *arXiv:2209.07028*, 2022.

[9] David Maxwell Chickering. Optimal structure identification with greedy search. *Journal of machine learning research*, 3(Nov):507–554, 2002.

[10] C. Chow and C. Liu. Approximating discrete probability distributions with dependence trees. *IEEE Transactions on Information Theory*, 14(3):462–467, 1968.

[11] Gregory C. Chow. Tests of equality between sets of coefficients in two linear regressions. *Econometrica*, 28(3):591–605, 1960.

[12] Thomas M. Cover and Joy A. Thomas. *Elements of Information Theory (Wiley Series in Telecommunications and Signal Processing)*. Wiley-Interscience, USA, 2006.

[13] Sanjoy Dasgupta. Learning polytrees. In *Proceedings of the Fifteenth Conference on Uncertainty in Artificial Intelligence*, pages 134–141. Morgan Kauffman Publishers, 1999.

[14] Atray Dixit, Oren Parnas, Biyu Li, Jenny Chen, Charles P. Fulco, Livnat Jerby-Arnon, Nemanja D. Marjanovic, Danielle Dionne, Tyler Burks, Raktima Raychowdhury, Britt Adamson, Thomas M. Norman, Eric S. Lander, Jonathan S. Weissman, Nir Friedman, and Aviv Regev. Perturb-seq: Dissecting molecular circuits with scalable single-cell rna profiling of pooled genetic screens. *Cell*, 167(7):1853–1866.e17, 2016.

[15] Mathias Drton, Bernd Sturmfels, and Seth Sullivant. *Lectures on Algebraic Statistics*, volume 39 of *Oberwolfach Seminars*. Springer, 2009.

[16] David Edwards, Gabriel Abreu, and Rodrigo Labouriau. Selecting high-dimensional mixed graphical models using minimal AIC or BIC forests. *BMC Bioinformatics*, 11(1), 2010.

[17] Jalal Etesami, Negar Kiyavash, and Todd Coleman. Learning Minimal Latent Directed Information Polytrees. *Neural Computation*, 28(9):1723–1768, 09 2016.

[18] Hamid Fehri, Ali Gooya, Yuanjun Lu, Erik Meijering, Simon Johnston, and Alejandro Frangi. Bayesian polytrees with learned deep features for multi-class cell segmentation. *IEEE Transactions on Image Processing*, PP, 01 2019.

[19] Gery Geenens and Pierre Lafaye de Micheaux. The hellinger correlation. *Journal of the American Statistical Association*, 117(538):639–653, 2022.

[20] AmirEmad Ghassami, Saber Salehkaleybar, Negar Kiyavash, and Kun Zhang. Learning causal structures using regression invariance. In I. Guyon, U. Von Luxburg, S. Bengio, H. Wallach, R. Fergus, S. Vishwanathan, and R. Garnett, editors, *Advances in Neural Information Processing Systems*, volume 30. Curran Associates, Inc., 2017.

[21] Malay Ghosh. Exponential tail bounds for chisquared random variables. *Journal of Statistical Theory and Practice*, 15(2):35, 2021.

[22] Niels Grttemeier, Christian Komusiewicz, and Nils Morawietz. On the parameterized complexity of polytree learning. In Zhi-Hua Zhou, editor, *Proceedings of the Thirtieth International Joint Conference on Artificial Intelligence, IJCAI-21*, pages 4221–4227. International Joint Conferences on Artificial Intelligence Organization, 2021.

[23] Alexander Hägele, Jonas Rothfuss, Lars Lorch, Vignesh Ram Somnath, Bernhard Schölkopf, and Andreas Krause. Bacadi: Bayesian causal discovery with unknown interventions. *arXiv:2206.01665*, 2022.

[24] Alain Hauser and Peter Bühlmann. Characterization and greedy learning of interventional markov equivalence classes of directed acyclic graphs. *J. Mach. Learn. Res.*, 13(1):24092464, aug 2012.

[25] Alain Hauser and Peter Bhlmann. Jointly interventional and observational data: estimation of interventional Markov equivalence classes of directed acyclic graphs. *J. R. Stat. Soc. Ser. B. Stat. Methodol.*, 77(1):291–318, 2015.

[26] Christina Heinze-Deml, Jonas Peters, and Nicolai Meinshausen. Invariant causal prediction for nonlinear models. *Journal of Causal Inference*, 6(2):20170016, 2018.

[27] Patrik Hoyer, Dominik Janzing, Joris M. Mooij, Jonas Peters, and Bernhard Schölkopf. Nonlinear causal discovery with additive noise models. In *Advances in Neural Information Processing Systems*, volume 21. Curran Associates, Inc., 2008.

[28] Amin Jaber, Murat Kocaoglu, Karthikeyan Shanmugam, and Elias Bareinboim. Causal discovery from soft interventions with unknown targets: Characterization and learning. In *Advances in Neural Information Processing Systems*, volume 33. Curran Associates, Inc., 2020.

[29] Martin E. Jakobsen, Rajen D. Shah, Peter Bhlmann, and Jonas Peters. Structure learning for directed trees. *Journal of Machine Learning Research*, 23(159):1–97, 2022.

[30] Markus Kalisch and Peter Bühlmann. Estimating high-dimensional directed acyclic graphs with the PC-algorithm. *Journal of Machine Learning Research*, 8(22), 2007.

[31] Joseph B. Kruskal, Jr. On the shortest spanning subtree of a graph and the traveling salesman problem. *Proc. Amer. Math. Soc.*, 7:48–50, 1956.

[32] Svante Linusson, Petter Restadh, and Liam Solus. On the edges of characteristic imset polytopes. *arXiv:2209.07579*, 2022.

[33] Xingmei Lou, Yu Hu, and Xiaodong Li. Linear polytree structural equation models: Structural learning and inverse correlation estimation. *arXiv:2107.10955*, 2021.

[34] Marloes Maathuis, Mathias Drton, Steffen Lauritzen, and Martin Wainwright, editors. *Handbook of Graphical Models*. Chapman & Hall/CRC Handbooks of Modern Statistical Methods. CRC Press, Boca Raton, FL, 2019.

[35] Ehsan Mokhtarian, Sina Akbari, AmirEmad Ghassami, and Negar Kiyavash. A recursive Markov boundary-based approach to causal structure learning. In Thuc Duy Le, Jiuyong Li, Greg Cooper, Sofia Triantafyllou, Elias Bareinboim, Huan Liu, and Negar Kiyavash, editors, *Proceedings of The KDD'21 Workshop on Causal Discovery*, volume 150 of *Proceedings of Machine Learning Research*, pages 26–54. PMLR, 15 Aug 2021.

[36] Ehsan Mokhtarian, Sina Akbari, Fateme Jamshidi, Jalal Etesami, and Negar Kiyavash. Learning Bayesian networks in the presence of structural side information. *Proceedings of the AAAI Conference on Artificial Intelligence*, 36(7):7814–7822, Jun. 2022.

[37] Ehsan Mokhtarian, Mohmmadsadegh Khorasani, Jalal Etesami, and Negar Kiyavash. Novel ordering-based approaches for causal structure learning in the presence of unobserved variables. *Proceedings of the AAAI Conference on Artificial Intelligence*, 37(10):12260–12268, Jun. 2023.

[38] Joris M. Mooij, Sara Magliacane, and Tom Claassen. Joint causal inference from multiple contexts. *J. Mach. Learn. Res.*, 21(1), jan 2020.

[39] William H Press. *Numerical recipes 3rd edition: The art of scientific computing*. Cambridge university press, 2007.

[40] Heinz Prfer. Neuer Beweis eines Satzes ber Permutationen. *Archiv der Mathematischen Physik*, 27:742–744, 1918.

[41] George Rebane and Judea Pearl. The recovery of causal poly-trees from statistical data. In *Int. J. Approx. Reason.*, 1987.

[42] Thomas Richardson and Peter Spirtes. Ancestral graph Markov models. *The Annals of Statistics*, 30(4):962–1030, 2002.

[43] Karen Sachs, Omar Perez, Dana Pe'er, Douglas A. Lauffenburger, and Garry P. Nolan. Causal protein-signaling networks derived from multiparameter single-cell data. *Science*, 308(5721):523–529, 2005.

[44] Firoozeh Sepehr and Donatello Materassi. An algorithm to learn polytree networks with hidden nodes. In H. Wallach, H. Larochelle, A. Beygelzimer, F. d'Alché-Buc, E. Fox, and R. Garnett, editors, *Advances in Neural Information Processing Systems*, volume 32. Curran Associates, Inc., 2019.

[45] Shohei Shimizu, Patrik O. Hoyer, Aapo Hyvärinen, and Antti Kerminen. A linear non-Gaussian acyclic model for causal discovery. *J. Mach. Learn. Res.*, 7:2003–2030, 2006.

[46] L Solus, Y Wang, and C Uhler. Consistency guarantees for greedy permutation-based causal inference algorithms. *Biometrika*, 108(4):795–814, 01 2021.

[47] Peter Spirtes, Clark Glymour, and Richard Scheines. *Causation, prediction, and search*. Adaptive Computation and Machine Learning. MIT Press, Cambridge, MA, second edition, 2000.

[48] Chandler Squires and Caroline Uhler. Causal structure learning: A combinatorial perspective. *Foundations of Computational Mathematics*, 2022.

[49] Chandler Squires, Yuhao Wang, and Caroline Uhler. Permutation-based causal structure learning with unknown intervention targets. In *Conference on Uncertainty in Artificial Intelligence*, pages 1039–1048. PMLR, 2020.

[50] Luis Enrique Sucar, Joaquín Pérez-Brito, J Carlos Ruiz-Suárez, and Eduardo Morales. Learning structure from data and its application to ozone prediction. *Applied Intelligence*, 7:327–338, 1997.

[51] Seth Sullivant, Kelli Talaska, and Jan Draisma. Trek separation for Gaussian graphical models. *The Annals of Statistics*, 38(3):1665–1685, 2010.

[52] Toshihisa Toyoda. Use of the Chow test under heteroscedasticity. *Econometrica*, 42(3):601–608, 1974.

[53] D. Tramontano, L. Waldman, and E. Duarte. Learning linear Gaussian polytrees with interventions. `https://github.com/emduart2/Polytrees`, 2023.

[54] Daniele Tramontano, Anthea Monod, and Mathias Drton. Learning linear non-Gaussian polytree models. In *Proceedings of the Thirty-Eighth Conference on Uncertainty in Artificial Intelligence*, volume 180 of *Proceedings of Machine Learning Research*, pages 1960–1969. PMLR, 2022.

[55] Yuhao Wang, Liam Solus, Karren Yang, and Caroline Uhler. Permutation-based causal inference algorithms with interventions. In *Advances in Neural Information Processing Systems*, volume 30. Curran Associates, Inc., 2017.

[56] K. D Yang, A. Katcoff, and C. Uhler. Characterizing and learning equivalence classes of causal dags under interventions. In *Proceedings of the 35th International Conference on Machine Learning*, volume 80 of *Proceedings of Machine Learning Research*, pages 5541–5550. PMLR, 10–15 Jul 2018.

[57] Alessio Zanga, Elif Ozkirimli, and Fabio Stella. A survey on causal discovery: Theory and practice. *International Journal of Approximate Reasoning*, 151:101–129, 2022.

[58] Mazad S. Zaveri and Dan Hammerstrom. Cmol/cmos implementations of bayesian polytree inference: Digital and mixed-signal architectures and performance/price. *IEEE Transactions on Nanotechnology*, 9(2):194–211, 2010.